MATERIALS AND SEMICONDUCTOR PHYSICS
STOCKHOLM 2003

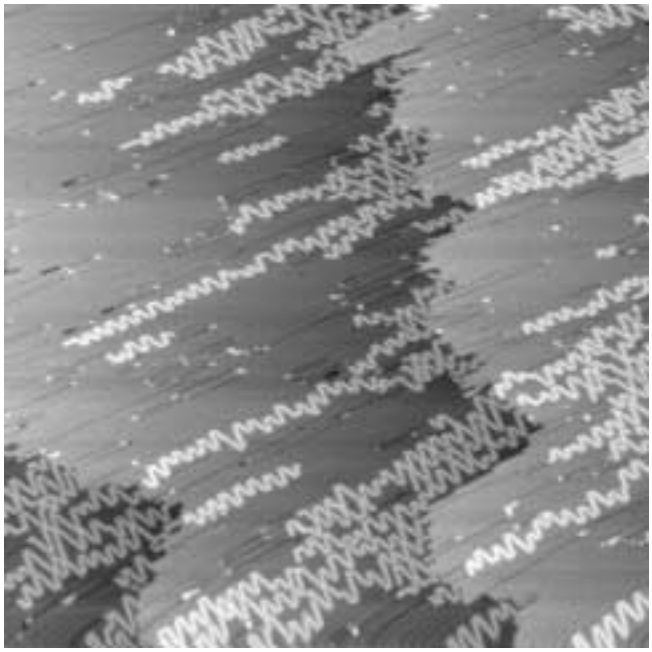

Molecular Level Studies of the Metal/Atmosphere Interface

Doctoral Thesis

Jonas Weissenrieder

Molecular Level Studies of the Metal/Atmosphere Interface

Jonas Weissenrieder

Materials and Semiconductor Physics
Kungliga Tekniska Högskolan
Stockholm

The figure on the cover shows a STM image of one dimensional zigzag sulfur chains on Fe(110).

Molecular Level Studies of the Metal/Atmosphere interface

Materials and Semiconductor Physics
KTH, Royal Institute of Technology
Stockholm
Sweden

TRITA-FYS 3076
ISBN 91-7283-399-8

Abstract

The chemistry and physics involved at the metal/atmosphere interface is interesting both from a fundamental and an applied perspective. Since iron is the most important of all metals this interface is of particular interest. The objective with this thesis is to obtain new information on a molecular level of the iron/atmosphere interface with a special emphasis on the initial atmospheric corrosion.

The work presented herein combines a large variety of different analytical surface science techniques. Both ultra high vacuum and ambient pressure investigations were conducted with single crystals as well as polycrystalline samples.

The interaction of segregated sulfur with a Fe(110) surface was investigated by means of atomically resolved scanning tunneling microscopy (STM). A large variety of high and low coverage reconstructions were reported. Comparable studies of oxygen adsorption on the same surface were also completed. Similar to the sulfur experiments, oxygen induced a number of low coverage reconstructions. At higher coverage, oxide formation was observed and ordered oxides could be fabricated at elevated temperatures.

The oxygen interaction with Fe(110) and Fe(100) surfaces were also investigated with synchrotron radiation based photoelectron spectroscopy. Detailed information of the initial adsorption and subsequent oxidation was obtained. The Fe 2p core level of the clean Fe(110) surface was subject to further investigations because of its complicated line profile that was interpreted as an exchange split of the final state.

Iron exposed to humidified air with low concentrations of sulfur dioxide (SO_2) shows a surprisingly passive behavior. The measured mass gain was significantly lower than that of a copper sample exposed in the same environment. In-situ

techniques such as atomic force microscopy (AFM), quartz crystal microbalance (QCM) and infrared reflection absorption spectroscopy (IRAS) showed little or no corrosion. Initiation of corrosion was observed upon introduction of additional oxidants. The conclusion drawn challenge the established model for formation and growth of sulfate nests. The condition and formation of sulfate nests are discussed in view of the generated *in-situ* observations.

During further experiments, iron was exposed to humid air and sodium chloride aerosols. The surface was investigated with *in-situ* techniques, which provided new useful information. A high corrosion rate was observed and the corrosion attacks form filaments characteristic of filiform corrosion. A schematic model for propagation of the corrosion filaments was proposed.

Filiform corrosion was observed on aluminum surfaces as well. The corroded surfaces were investigated with synchrotron radiation based photoelectron microscopy and scanning over a filiform head revealed different oxidation states within the Al 2p spectrum. The microscopy data was interpreted as an enrichment of aluminum chloride containing compounds within the filiform corrosion head.

Preface

The experimental work presented in this thesis was performed at Materials and Semiconductor Physics (KTH), Div. Corrosion Science (KTH), at MAX-lab in Lund and at Vienna University of Technology.

List of Publications

The following papers are presented in this thesis:

I. J. Weissenrieder, M. Göthelid, G. LeLay and U.O. Karlsson,
Investigation of the Surface Phase Diagram of Fe(110)-S, *Surf. Sci.* **515**, 135-142 (2002)

II. J. Weissenrieder, M. Göthelid, H. von Schenck, M. Månsson, O. Tjernberg and U.O. Karlsson,
Oxygen Structures on Fe(110),
Surf. Sci. **527**, 163-172 (2003)

III. J. Weissenrieder, P. Palmgren, T. Claesson, M. Göthelid, U.O. Karlsson,
Initial Oxidation of Fe(100) and Fe(110),
Manuscript

IV. J. Weissenrieder, C. Leygraf, M. Göthelid and U.O Karlsson,
Photoelectron Microscopy of Filiform Corrosion of Aluminum,
Accepted for publication in Appl. Surf. Sci.

V. J. Weissenrieder and C. Leygraf,
***In-situ* Studies of Filiform Corrosion of Iron**,
Submitted to J. Electrochem. Soc.

VI. J. Weissenrieder and C. Leygraf,
***In-situ* Studies of the Initial Atmospheric Corrosion of Iron**,
Outdoor Atmospheric Corrosion, ASTM STP 1421, H.E. Townsend, Ed., ASTM International, West Conshohocken, PA, 127-138 (2002)

VII. Ch. Kleber, J. Weissenrieder, M. Schreiner and C. Leygraf,
Comparison of the Early Stages of Corrosion of Copper and Iron Investigated by *In-situ* TM-AFM,
Appl. Surf. Sci. **193/1-4**, 245-253 (2002)

VIII. J. Weissenrieder, C. Kleber, M. Schreiner and C. Leygraf,
***In-situ* Studies of Sulfate Nest Formation on Iron**,
Manuscript

The following papers have resulted from work that is not presented in the thesis:

IX. Y. Itoh, T. Suzuki, M. Birukawa and J. Weissenrieder,
Magnetic and Magneto-Optical Properties of TbFeCo/(Pd, Pt) Multilayers Optimized for Short Wavelength Recording,
J. Appl. Phys. **85**, 5091 (1999)

X. Y. Itoh, J. Weissenrieder and T. Suzuki,
Magnetic and Magneto-Optical Properties of TbFeCo/(Pt, Pd, NdCo) Multilayers,
J. Magn. Soc. Jpn., **23**, 1081 (1999)

XI. Y. Itoh, G.N. Phillips, T. Suzuki and J. Weissenrieder,
Proc., Enhancement of Magneto-optical Effects through Polarized Pt and Pd in TbFeCo/(Pt, Pd) Multilayers,
J. Magn. Soc. Jpn. **23** (Suppl. No. S1), 55 (1999).

XII. E. Janin, S. Ringler, J. Weissenrieder, T. Åkermak, U.O. Karlsson and M. Göthelid,
Adsorption and Bonding of Propene and 2-Butenal on Pt(111),

Surf. Sci. **482-485**, 83 (2001)

XIII. M. Sinner-Hettenbach, M Göthelid, J. Weissenrieder, H. Von Schenk, T. Weiss, N. Barsan and U Weimar,
Oxygen-deficient SnO_2(110): A STM, LEED and XPS study, *Surf. Sci.* **477**, 50 (2001)

XIV. E. Janin, H. von Schenck, S. Ringler, J. Weissenrieder, T. Åkermak, U.O. Karlsson, D. Nordlund, H. Ogasawara and M. Göthelid,
Adsorption and Bonding of 2-Butenal on Sn/Pt Surface Alloys,
to be published in Journal of Catalysis

XV. J. Weissenrieder, J. Österman and C. Leygraf,
***In-situ* Studies of the Initial Atmospheric Corrosion of Iron - Influence of SO_2, NO_2 and NaCl**,
Electrochem. Soc. Proc. 22, 733-740 (2001)

XVI. H. von Schenck, J. Weissenrieder, S. Helldén, M. Göthelid, **Reactions of Iodobenzene on Pd(110) and Pd(111)**,
Appl. Surf. Sci., 1, 9813 (2003)

XVII. H. von Schenck, J. Weissenrieder, B. Åkermark, and M. Göthelid,
Iodine induced structures on Pd(110), Pd(111) and Pt(110) surfaces,
Manuscript

XVIII. P. Palmgren, K. Szamota-Leandersson, J. Weissenrieder, T. Claesson, O. Tjernberg, U.O. Karlsson, M.C. Qian, S. Mirbt and M. Göthelid,
Adsorption Site, Chemical Reaction and Electronic Structure of InAs(111)-Co Surfaces,
Manuscript

Contents

1 Introduction

1.1 Surfaces and Surface Physics

Both solids and liquids must have surfaces or interfaces and these exhibit some remarkable physical and chemical properties. Surface phenomena have been, and will continue to be among the most fascinating subjects in both fundamental and applied science. In the present work the attention has been focused on solid surfaces and their interaction with, predominantly, the gas phase.

Much of our understanding of solids is based on the fact that they often are perfectly periodic in three dimensions. Basic research in solid state science is increasingly confronted with problems related to surface effects, since all solids have boundaries. Our knowledge of surface properties is, however, still inferior to that of bulk phases due to the additional experimental and theoretical complications associated with the absence of the third dimension.

At a fundamental level surfaces are of great interest because they represent a rather special kind of defect in the solid state. When cleaving a crystal into two, new surfaces are formed and the physical difference between the initial and final state is these two surfaces. All surfaces are energetically unfavorable in that they have a positive free energy of formation. A simple reason for why this must be the case comes from considering that the formation of the new surfaces requires that bonds have to be broken between atoms on either side of the cleavage plane in order to split the solid. Breaking bonds requires work to be done on the system, so the surface free

energy contribution to the total free energy of a system must therefore be positive.

In physics there exist two limiting cases when describing the properties of three dimensional matter: the ideal gas and the ideal solid. The former is composed of point particles, which interact only by elastic collisions. The latter consists of a strictly periodic arrangement of atoms forming a lattice without defects and impurities, extending to infinity in all three dimensions. In analogy with the ideal solid approach, a similar model of an ideal surface can be formed as a perfectly periodic arrangement of surface atoms in two dimensions. In experimental research, single crystal surfaces may serve as a corresponding model system.

Many investigations of surfaces are performed in ultra high vacuum (UHV). It is not generally the measurement techniques themselves that are pushing for UHV. The mean free path of electrons in UHV is far longer than needed and many techniques may be used at above atmospheric pressure [1]. Instead, it is the surfaces themselves that need this environment. In order to study the initial reaction of a gas with a surface the pressure has to be decreased, otherwise the reaction with the previously described broken bonds on the surface will happen too fast. As an example, every surface atom will, on average, interact with one molecule of the reaction gas every second at the pressure 10^{-6} Torr (~10^{-9} atmospheres). This means that if every such interaction would end up with a bond, one monolayer would be formed every second. In the case of clean surfaces this may sometimes be almost true, but as the surface reaction proceeds the process slows down when a protective layer covers the surface.

Perhaps the most widely quoted motivation for modern surface studies is the understanding of heterogeneous catalysis. It is the enhanced reaction rates in the presence of solid catalysis, the chemical behavior of surfaces, which is responsible for heterogeneous catalysis in e.g. ammonia synthesis [2]. Another area of interest involves photosynthesis, where the absorbtion of

sunlight and the reactions of water and carbon dioxide produce organic molecules and oxygen. High surface area systems, such as the green leaf, are most efficient to carry out photosynthesis [2]. Further, the degradation and corrosion of materials is an ever-ongoing process that costs billions of dollars each year worldwide. The annual costs for corrosion is usually corresponding to a few percent of the gross national product [3].

A current trend in surface studies is towards *in-situ* analysis, i.e. investigation of surface properties during reaction. An obvious advantage of such investigations is the increased control of the environmental conditions of the system and decreased risk for discrepancy as surface properties may change with the surrounding environment.

The objective with molecular level investigations is to increase our knowledge of the system of interest. In order to gain new fundamental information it is vital to understand the interaction between the smallest particles (atoms and molecules) involved. In silicon technology it is possible to control extremely low dopant levels and grow structures on a nm scale. If the same knowledge and understanding would be available in other systems, it is not far fetched to believe that this would make an enormous impact on the advancement of the technology and our society. What would the world be like if we did not have computers?

1.2 Physisorption, chemisorption and desorption

All surfaces exposed to a gas, atmosphere, will have some kind of interaction with the gas phase. This interaction can usually be described within the terms adsorption and desorption. Adsorption is adhesion of molecules or atoms from the gas phase on the surface. This will occur on both solid and liquid interfaces. Desorption can be described as a release of atoms or molecules from the surface to the gas phase. In order to improve the fundamental understanding of how surfaces interact with the surrounding

environment, molecular level studies of this process have to be performed. Within the term adsorption, it is possible to distinguish between two types of interaction with surfaces: physisorption and chemisorption.

1.2.1 Physisorption

Molecules or atoms physisorbed on a surface can be characterized by a low bonding energy (5-100 meV) and a rather large equilibrium distances (3-10 Å) to the surface. The physisorption process will weakly perturb the electronic structure of the adsorbate and the substrate. An attractive force is created due to correlated charge fluctuations in the bonding partner, i.e., mutually induced dipole moments. In physisorption it is a valid assumption to consider the substrate as uniform jellium, since the long bond lengths diminish site dependent variations on the surface. Further, since the bonding is relatively weak, physisorption of molecules or atoms will generally occur at low sample temperatures. In ambient atmosphere, at room temperature, a thin layer of physisorbed water covers all surfaces [3,4]. This thin water layer plays an essential role in the interaction between the surface and the ambient atmosphere.

1.2.2 Chemisorption

In chemisorption the valence electron wave function overlap between the substrate and adsorbate results in the formation of new bonding orbitals. Compared to physisorption the bond energies are relatively high, above 1 eV, and involve short bond distances. Chemisorption is an exothermic reaction and the substrate lattice absorbs heat or energy emitted in the process as phonons. The energy absorption may be detected as an increased sample temperature in calometric measurements [5]. In contrast to physisorption, the substrate jellium assumption is no longer suitable, since the potential varies significantly from different sites on the surface due to the short bond distance. In a surface potential map every minimum will correspond to an

adsorption site. The locations of these sites are highly dependent on the local geometric and electronic structure.

In chemisorption of molecules, the rearrangement of the electronic structure may cause dissociation. In dissociation the adsorbed molecule breaks apart and a formation of new adsorbate species take place. Dissociative adsorption of water occurs on almost all metals at room temperature [4]. The dissociative adsorption of water on Fe(100) has been reported to occur already at T < 100 K and the dissociated OH-group will start to further decompose in O and H at temperatures slightly above room temperature [6].

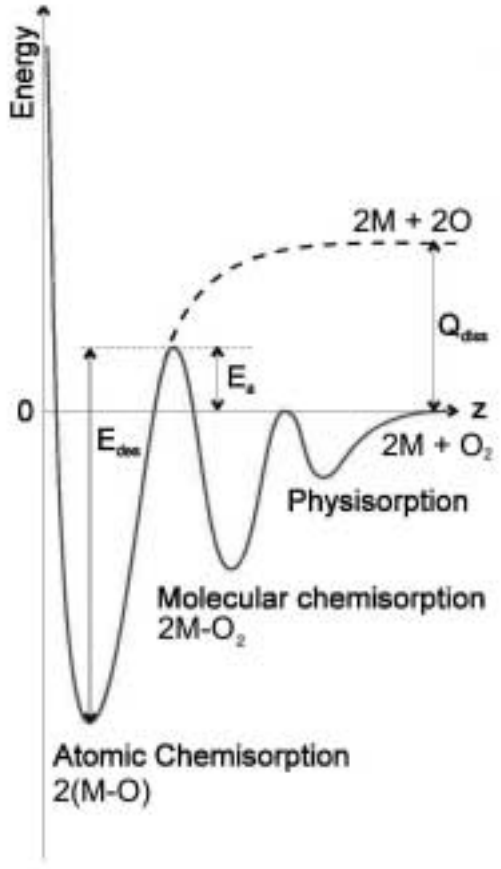

Figure 1.1 Illustration of adsorption of an O_2 molecule on a metal surface.

Figure 1.1 is a schematic illustration of the gas surface interaction potential for the diatomic molecule O_2 approaching a metal surface. In this one-dimensional diagram three sequential adsorption wells are depicted, corresponding to the three types of adsorption steps presented above. The first step, outermost and shallowest, correspond to the physisorption

potential well and in the well midway to the surface the O_2 molecule is chemisorbed in molecular form. When reaching the innermost and deepest potential well the O_2 molecule has dissociated and the potential represents chemisorption of atomic O. The initial decrease in energy when an O_2 molecule approaches the metal surface is due to the attractive interaction between O_2 and the surface. The sharp increase of the potential close to the iron surface originates from the increased Pauli repulsion.

When atoms and molecules adsorb on a surface they will be influenced by the interaction with other adsorbates. This mutual interaction is of great importance for the reactions taking place on the surface and can be attributed to one or many of the following interaction mechanism: van-der-Waals attraction due to the correlated charge fluctuation, orbital overlap of the neighboring adsorbates, dipole forces from permanent dipole moments of the molecules or substrate mediated interaction. The interaction of dipole forces can be seen in multilayer adsorption of water on metal surfaces as the formation of the electrochemical double layer [7]. The substrate mediated interaction is due to modification of the electronic structure of the substrate by strongly chemisorbed species, which results in changes in the properties of neighboring adsorption sites. Strong attractive interaction between adsorbates can lead to the formation of islands, whereas for dominating repulsion an even distribution of the atoms or molecules is most natural.

The local environment of the metallic surface atoms is clearly modified by chemisorption of molecules on the surface. In a simple model of a clean metal surface the surface atoms experience quasi-infinite metal bulk symmetry in one direction and vacuum in the other direction. The formation of a chemical bond between the metal surface atom and the adsorbate change the local density of states experienced by the metal atom and thus it is likely that the chemisorption process modify the geometric structure of the clean surface. This modified surface geometry will be adapted to the new surface configuration with an adsorbate present on the surface and consequently the symmetry experienced by the surface metal atom is rather

different from the clean surface. Numerous examples of adsorbate induced surface reconstructions are given in the literature [8-10]. A dramatic example is given by the oxidation of Al(111) where a new metallic state bound to only three Al atoms is formed [11].

1.2.3 Desorption

When an adsorbed molecule or atoms bond to the substrate breaks, it may desorb from the surface. This breaking of bonds and subsequent desorption can be caused by thermal excitation, by adsorption of other species and by excitation of electronic or vibrational states. The control of desorption and desorption rate is of great technological importance, for instance in heterogeneous catalysis. Further, the desorption mechanism of atoms and molecules from surfaces is frequently used in desorption spectroscopies, such as temperature programmed desorption (TPD) [1,12-13].

References

1. D.P Woodruff, T.A. Delchar, *Modern techniques of surface science*, Cambridge University Press, Cambridge (1990)
2. G.A. Somorjai, *Introduction to surface chemistry and catalysis*, John Wiley & Sons, New York (1994)
3. C. Leygraf and T.E. Graedel, *Atmospheric corrosion*, John Wiley & Sons, New York (2000)
4. M.A. Henderson, *Surf. Sci. Rep.*, **46**, 1 (2002)
5. A. Stuck, C.E. Wartnaby, Y.Y. Yeo, J.T. Stuckless, N. Al-Sarraf and D.A. King, *Surf. Sci.*, **349**, 229 (1996)
6. P.A Thiel and T.E. Madey, *Surf. Sci. Rep.*, **7**, 211 (1987)
7. J. O'M. Bockris and A. K. N. Reddy, *Modern electrochemistry*, volume 2, Plenum Press, New York (1970)
8. M. Bernasconi and E. Tosatti, *Surf. Sci. Rep.*, **17**, 363 (1993)
9. Š. Pick, *Surf. Sci. Rep.*, **12**, 101 (1991)

10. D.P. Woodruff, *J. Phys. Condens. Matter*, **6** 6067 (1994)
11. C. Berg, S. Raaen, A. Borg, J.N. Andersen, E. Lundgren, R. Nyholm, *Phys. Rev. B*, **47**, 13063 (1993)
12. G. Ertl, J. Küppers, *Low energy electrons and surface chemistry*, Weinheim, Germany (1985)
13. H. Lüth, *Surfaces and Interfaces of Solid Materials*, 3rd Edition, Springer-Verlag, Berlin Heidelberg New York (1997)

2 Iron and its alloys

Quite frequently I have been asked what the objectives are to perform molecular level investigations of iron surfaces. A simple answer would, of course, be that it is of a fundamental interest to gain an improved knowledge of almost any thing at any time. But iron really has an outstanding position as the most important metal in our society. It is the cheapest, most abundant and useful of all metals [1]. Consequently, an improved knowledge of this system will be interesting from many points of view.

The chemistry of iron frequently shows unforeseen properties that are challenging to explain. An example is the famous more than 1600 years old iron pillar monument in Delhi. This solid shaft of wrought iron is about 7¼ meters high and 40 cm in diameter and is one of the oldest known iron constructions in the world. Corrosion to the pillar has been minimal even though it has been exposed to the ambient weather since its erection [2].

Figure 2.1 The iron pillar monument in Delhi.

Iron is an important catalyst, especially in the ammonia process. Iron sulfides are natural catalysts that promote ammonia formation even at atmospheric pressures [3].

In a recent theory of the origin of life iron sulfide (FeS_2) honeycombs have been proposed to be an ideal place for life to start [4]. The honeycomb structure has pockets some hundred micrometers across and would have been situated near hot springs on the ocean floor. The iron sulfide speeds up the reactions that join inorganic molecules into organic ones – some bacteria still use it. The hot water flowing out of springs and into the honeycomb's holes is rich in the raw ingredients for these reactions, such as ammonia and carbon monoxide. Bacteria can nourish on such compounds [4].

In the form of steel, iron is a frequently used construction material. In all its different exposure environments iron experience a lot of different problems such as corrosion [5-7], metal dusting [8], fatigue [9] etc.

Further, iron is a carrier of magnetism. It is its unpaired electrons in the d-band that is the origin of the magnetic moment. Among the 3d transition metals, iron possesses the highest magnetic moment [10,11]. Consequently iron is frequently used in magnetic applications, such as magnetic storage, permanent magnets and may play an important role in future applications such as spin-memories and spin-transistors.

Iron (or stainless steel) may also be used, as implants, inside our bodies. It is considered to be biocompatible and is used for instance as hip joints. Actually steel is one of the most commonly used metal implants within our body [12-13].

There are 200 billions of red blood cells within an adult man's bloodstream. They have a life length of approximately 120 days, consequently over one million new blood cells have to be produced every minute. All of theses blood cells contain the indispensable hemoglobin with purpose to transport oxygen

to all the cells within the body. In the functional group iron plays an important role as the electron transfer element in the redox processes with oxygen [14]. It is also involved in the formation of chlorophyll, even though it is not a part of that substance [15].

By now, most people have lost their interest a long time ago and therefore the fundamental interest answer is often the easiest answer to give.

2.1 Atmospheric corrosion of iron

The interaction between a metal and its surrounding atmosphere is of profound importance for many naturally occurring or technically important processes, for instance the degradation of scrap metals in the environment, life length of various construction materials or magnetic storage materials limited by corrosion. Atmospheric corrosion has been noticed ever since mankind started to use metals and the knowledge that a metal degrade into a mineral have long been well known. However, it was not until the beginning of the 20th century that atmospheric corrosion became a scientific discipline. At this time Vernon began to systematically study the influence of humidified air at different relative humidity and sulfur dioxide concentration on the atmospheric corrosion by gravimetric measurements [16-17].

Ever since then, the field has constantly developed and today all phases involved in the reaction process must be considered, as schematically illustrated in Figure 2.2. As a consequence, chemists, electrochemists, physicists and material scientists are all involved in the research field and therefore atmospheric corrosion can truly be called an interdisciplinary field of science.

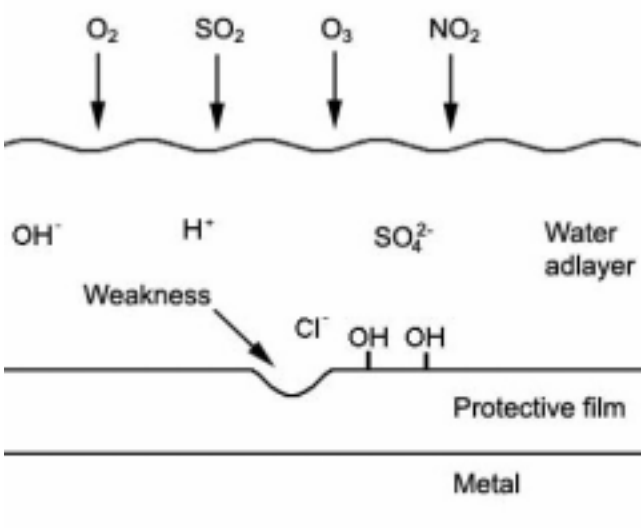

Figure 2.2. Schematic picture of the metal-atmosphere interface.

Interaction of water with surfaces under vacuum conditions has been extensively studied by many techniques, a comprehensive review has been compiled by Henderson [18], and numerous studies have been investigating the adsorption of water on metal surfaces under atmospheric pressure [19-21]. In addition, several different research groups [22-25] have examined the role of water in atmospheric corrosion in combination with different gases or other corrosion stimulators in laboratory experiments. The corrosion products formed in field environments and the sequence for the formation has also been studied [26-29].

However, well-defined studies of the processes occurring at the metal-atmosphere interface are difficult to perform and many questions especially regarding the initiation of corrosion are still unanswered. The complete mechanism of the corrosion process must be known in order to perform accurate accelerated tests, something of growing importance.

It is well known since the early studies of Vernon that certain so called corrodents accelerate the atmospheric corrosion of iron. The presence of humidified air and SO_2 have been described as vital, some studies even claim that no significant rusting occurs if SO_2 is not present [30]. The concentrations of SO_2 in the atmosphere have decreased during the last

decades and consequently its relative importance has decreased [31]. In this study we have focused our research on the interaction of iron surfaces with SO_2 and humidified air combined with other corrosion accelerating pollutants such as nitrogen dioxide (NO_2), ozone (O_3) and sodium chlorides (NaCl). Most of the SO_2 and NO_2 in the atmosphere originate from the combustion of fossilized fuels, while the main source for NaCl is the oceans. Each year, wave action on the Earth's oceans injects an estimated 10^{12} kg of sea salt into the atmosphere as an aerosol of microscopic aqueous droplets [32].

2.2 Electrochemistry and corrosion

Already as a result of Vernon's early work [16-17] it became obvious that the atmospheric corrosion of iron has to be considered as part of the electrolytic corrosion, therefore strongly depending on the presence of electrolyte layers on top of the surface. This explains both the importance of high humidity as the importance of atmospheric impurities, which later represent the ionic constituents of the electrolytic phase.

During these early studies it was recognized that the atmospheric corrosion of steel is by no means a spatially homogenous reaction but takes place in local reaction sites visible even by low magnification. One of the earliest attempts to explain this localized electrochemistry was made by Evans in the thirties when he described his famous water droplet deposited on an iron surface [33]. His explanation, which is still valid, is based on the difference in transport kinetics for molecular oxygen between the outer and inner part of the droplet. Due to the high rate of oxygen reduction in the outer part the iron surface passivates, whereas the inner part shows predominantly metal dissolution and therefore an acidic electrolyte. In this model, separated anodic and cathodic areas on the iron surface were introduced.

2.3 Initiation of corrosion

Passive layers are formed on many reactive metals. If these films have semiconducting properties, as for iron, they will grow up to a few nanometers in thickness to the potential of oxygen evolution. The electric field strength within the passive layer of some nanometers is in the order of some 10^6 V/cm. This high field strength enables the migration of ions through the film at room temperature at a measurable level in the region of corresponding current densities of some few $\mu A/cm^2$ or less [7]. It is the stability of these passive layers that provide aluminum with its great corrosion resistance and the frequent break down of the same films that will initiate a corrosion attack on iron. Since our interest is in the initial corrosion mechanisms I will briefly describe some passive film break down mechanisms proposed in the literature.

In the adsorption theory, pits are formed as a result of the competitive adsorption of chloride ions and oxygen [34]. Pits develop at sites where oxygen adsorbed on the metal surface is displaced by chloride ions. The passivation of the surface is regarded as a dynamic process, i.e. continuous passivation and depassivation of the metal surface occur. It might therefore be assumed that on some uncovered sites of the surface, adsorption of Cl^- occurs, which leads to breakdown. However, the occurrence of a relatively long induction time is also observed and in such cases the theory would be difficult to substantiate.

There are many different theories describing penetration and migration of anions through the passive layers [35]. These theories have focused on the small diameter of Cl^- that enables permeation through the protective film. Breakdown of the film occurs when the aggressive anion reaches bare, or metallic, metal. This model also considers the first step leading to passivity breakdown as the aggressive anion adsorption on the oxide film. Pit initiation might be caused by the entry of anions, under the influence of an electrostatic field, across the film/solution interface when the field reaches a

critical value corresponding to the breakdown potential. Smaller ions more readily penetrate the lattice. The initial entry of anions is at the regions of the film corresponding to grain boundaries or other imperfections of the metal. The penetrating anions are not discharged since the anode potential is not sufficiently positive. They may travel through the passivating film as metal cations travel outward to meet them. Such a contaminated oxide film is a much better ion conductor than the original passivating oxide.

Water bound in the film is considered to play an important part in the pit initiation. Hydrated oxide films have a strong buffering ability that prevents film breakdown because of their good repairing action assured by the abundance of water molecules in the structure of the film [36]. In contrast a well-developed oxide, which has lost protons has less capacity to repair the film destroyed by Cl^-. Chloride ions that are adsorbed on the surface are thought to migrate through the film with the assistance of the electric field and replace water molecules. In this case no repairing of the film occurs. Alternatively, the reaction between metal ions and chloride ions surrounding the reaction site proceeds, thus forming solvated ions or salt-like films.

There are a few things contradicting the migration and penetration theory: The nucleation process is often too fast to be explained by migration through a continuous oxide film. Cl^- and O^{2-} have greater diameters than Fe^{3+}, so their transport should be less rapid. Pitting phenomena observed in SO_4^{2-} solutions cannot be explained the same way. The sulfate ion is too large to be able to penetrate the passive film [37].

Another important theory is considering the chemical dissolution in which it can be stated that a mechanism of passivity of iron should include consideration of the formation and existence of metal-anion complexes. Stable species inhibit corrosion while transient complexes accelerate corrosion. In sulfate solutions the cathodic process controls the corrosion of iron, but in chloride solutions Cl^- is directly involved in the anodic process. In neutral solutions, chlorides form iron chloride complexes that dissociate

and remove iron cations from the surface. The complexes are believed to involve three or four halide ions that jointly adsorb on the oxide film surface around a lattice cation, with one next to a surface anion vacancy for preference [7]. This theory is a popular description of the localized corrosion of aluminum.

Pits are thought to nucleate at defects in the film where the oxide thickness is smaller and the potential drop across the oxide/solution interface is higher. Localized damages of the surface oxide film is assumed to occur through chemisorption of Cl^- replacing O^{2-} och OH^- ions at the oxide surface and the formation of a two dimensional nucleus of chloride salt on the passivated metal surface. In the presence of aggressive anions, repassivation of these defects is prevented and pitting results [37].

The critical potential is less noble at Cl^- adsorption sites compared with Cl^- free sites on the film surface and is affected by the electronic properties of the passive film, hence by the electron acceptor levels introduced by anion adsorption as well as by defect induced electron levels. However, breakdown of the passive film does not necessarily lead to pitting. Pitting occurs only when a critical concentration of aggressive anions and a critical acidity is built up.

References

1. R. C. West, Ed., *Handbook of chemistry and physics*, CRC Press, Ohio (1975)
2. R. Balasubramaniam, *Corros. Sci.*, **42**, 2103 (2000)
3. G.A. Somorjai, *Introduction to surface chemistry and catalysis*, John Wiley & Sons, New York (1994)
4. W. Martin and M. Russell, Philosophical Transactions of the Royal Society B, **358**, 59 (2002)

5. C. Leygraf and T.E. Graedel, *Atmospheric corrosion*, John Wiley & Sons, New York (2000)
6. K. Barton, *Protection Against Atmospheric Corrosion*, John Wiley & Sons, New York (1976)
7. P. Marcus and J. Oudar, *Corrosion Mechanism in Theory and Practice*, Marcel Dekker, Inc. New York, USA (2002)
8. P. Szakalos, *Mechanisms of metal dusting on stainless steel*, KTH dissertation, ISBN 91-7283-260-6 (2002)
9. S. Suresh, *Fatigue of Materials*, Cambridge Univ. Press (1991)
10. C. Kittel, Introduction to solid state physics, Seventh edition, Wiley, Brisbane (1996)
11. N.W. Ashcroft and N.D. Mermin, *Solid state physics*, Saunders Collage CBS Publishing, Philadelphia (1988)
12. B. D. Ratner & A. S. Hoffman, F. J. Schoen, J. E. Lemons, Eds. *Biomaterials Science, An Introduction to Materials in Medicine*, Academic Press, UK, (1996)
13. J. A. Helsen, H. J. Breme, *Metals as Biomaterials*, John Wiley & Sons Ltd. (1998)
14. A. Lindgren and S. Jansson, *Pacemakern och hjärtat*, Siemens-Elema AB, ISBN 91 86068-16-4 (1992)
15. G. Hägg, *Allmän och oorganisk kemi*, Almqvist & Wiksell, Stockholm (1989)
16. W. H. J. Vernon, *Trans Faraday Soc.*, **19**, 839 (1923)
17. W. H. J. Vernon, *Trans Faraday Soc.*, **23**, 113 (1927)
18. M.A. Henderson, *Surf. Sci. Rep.*, **46**, 1 (2002)
19. S. Lee and R. W. Staehle, *Corrosion*, **53**, 33 (1997)
20. J. F. Dante and R. G. Kelly, *J. Electrochem. Soc.*, **140**, 1890 (1993)
21. S. P. Sharma, *J. Vac. Sci. Technol.*, **16**, 1557 (1978)
22. P. B. P. Phipps and D. W. Rice, *ACS. Symp. Ser 89*,, Am. Chem. Soc., Washington, DC, p 239 (1979)
23. S. Zakipour and C. Leygraf, *Br. Corros. J.*, **27**, 295 (1992)
24. P. Eriksson, L. G. Johansson and H. Strandberg, *J. Electrochem. Soc.*, **140**, 53 (1993)

25. R. E. Lobning, R. P. Frankenthal, J. D. Sinclair and M. Stratmann, *J. Electrochem. Soc.*, **141**, 2935 (1994)
26. T. Graedel, K. Nassau and J. P. Franey, *Corr. Sci.*, **27**, 639 (1987)
27. T. Graedel, *Corr. Sci.*, **27**, 721 (1987)
28. T. Graedel, *Corr. Sci.*, **27**, 741 (1987)
29. I. Odnevall and C. Leygraf, *J. Electrochem Soc.*, **142**, 3682 (1995)
30. U.R. Evans and C.A.J. Taylor, *Corros. Sci.*, **12**, 227 (1972)
31. J. Tidblad, V. Kucera, A.A. Mikhailov, J. Henriksen, K. Kreislova, T. Yates and B. Singer, *Outdoor Atmospheric Corrosion, ASTM STP 1421*, H.E. Townsend, Ed., American Society for Testing and Materials International, West Conshohocken, PA (2002)
32. P. Warneck, *Chemistry of the Natural Atmosphere* (Academic Press, New York (1988)
33. U.R. Evans, *Metallic Corrosion*, 166, London (1937)
34. H.H. Uhlig, J. Electrochem. Soc., **97**, 215C (1950)
35. U.R. Evans, J. Chem. Soc. London, page 1020 (1927)
36. G. Okamoto, Corros. Sci., 13, 471 (1973)
37. Z. Szklarska-Smialowska, *Pitting corrosion of metals*, National Association of Corrosion Engineers, Huston (1986)

3 Experimental Techniques

Within the work presented in this thesis a large number of different analytical surface science techniques have been used. The motive for employing a wide variety of techniques may be expressed in my belief that no technique is an island. With this I mean that information gained from using one technique almost always will be strengthened by complimentary information from other techniques. In this section, a short review of some of the utilized techniques will be presented.

3.1 Infrared Reflection Absorption Spectroscopy

Spectroscopy using infrared light has been used for approximately 100 years [1]. The development started with Michelson's invention of the interferometer for which he received the Nobel prize in 1907. Although it had an early start, it was not until the late 1960s that the infrared spectroscopy became widely spread and a commonly used method. The development of affordable computers made Fast Fourier Transformations of the interferogram feasible in the laboratory and thus calculations of the infrared spectra of the sample. One of the advantages of Fourier transform infrared (FTIR) spectroscopy and other photon in photon out techniques is that it can be used under atmospheric pressure in contrast to electron spectroscopic techniques where lower pressure is needed. The information depth spans from sub monolayer to ≈1 μm and a FTIR spectrometer is generally quite straightforward to operate. The drawbacks are mainly a poor lateral resolution ≈10 mm^2 and difficulties to interpret spectra and quantify the different species.

The physical principle of FTIR is that atoms within a molecule vibrate and the molecule can absorb a photon by activating a vibration. The number of dipole active vibration of a *gas phase* molecule is determined by its internal degrees of freedom and by the requirement of a non-zero dipole moment change associated with the vibration. A non-linear molecule with N atoms has 3N-6 (3N-5 for a linear molecule) internal degrees of freedom, when the translational (3) and rotational (3 for nonlinear, 2 for linear) motions are subtracted [2]. That is 3N-6 different vibrations within the molecule. In Figure 3.1, the possible vibrations of a gas phase SO_2 molecule are illustrated [3].

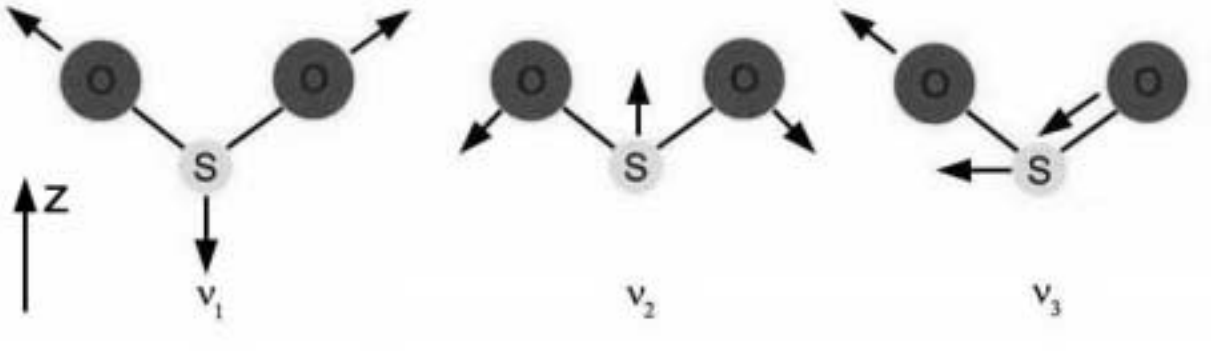

Figure 3.1. Schematic picture of the three fundamental vibrational modes of a gas phase SO_2 molecule; ν_1 (symmetric stretch), ν_2 (symmetric bend) and ν_3 (asymmetric stretch).

In the case of an adsorbed molecule, the number of vibrational modes is determined by the number of internal modes (3N-6) plus the number of frustrated rotational and translational modes. The latter are determined by the symmetry of the adsorption site [3]. The coordination of a molecule to a surface may cause a split of degenerated vibration modes due to loss of symmetry. It may also affect the vibration frequency.

A molecular vibration can interact with an oscillating electrical field of light. Since the wavelength of infrared light (≈1 μm) is many orders of magnitude larger than the size of a molecule (a few Å), the molecule will experience a uniform electric field. As an example, consider the ν_1 vibration of a SO_2 molecule in Figure 3.1. An electric field with an E-vector aligned with the z-

axis will move the positive sulfur atom downward, toward more negative z values, and the negative oxygen atoms upward. As the electric field oscillates it will tend to move the atoms upwards and downwards thereby causing a vibration in the molecule. If this vibration causes a change of the dipole moment, as in the example, the vibration is said to be infrared active and can absorb energy from the light, Figure 3.2. This absorption becomes efficient if the frequency of the oscillating electric field is close to the resonance frequency for the vibration and is proportional to the square of the change of dipole moment, $A \propto (\partial\mu/\partial Q_i)^2$ where μ is the dipole moment and Q_i is a normal coordinate. It should be stressed that a molecule does not have to be a dipole to absorb infrared light, it is enough that a change of dipole moment occurs.

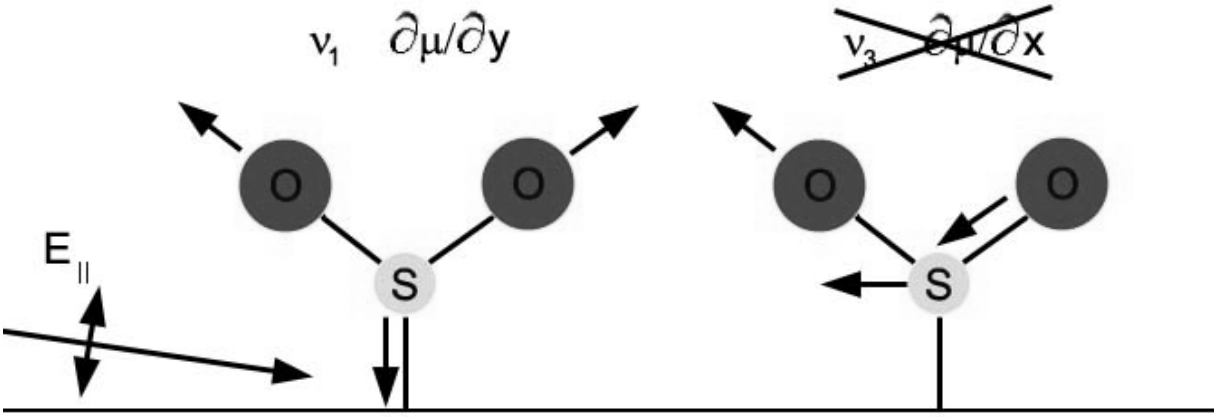

Figure 3.2. Schematic picture of the surface selection rule. A change of dipole moment must have a component perpendicular to the surface. The ν_1 vibration mode can interact and absorb the light, but ν_3 has its change of dipole moment parallel to the surface and is unable to interact.

In infrared reflection absorption spectroscopy (IRAS) the light is reflected against the sample surface. When light strikes a surface, the electrical field of the light can be divided into two perpendicular components. $E_{||}$ is located in the plane of incidence, parallel to the angel defined by the normal to the surface and the direction of the incoming light, and $E_{\perp}$ is perpendicular to the plane of incidence, parallel with the surface. Upon reflection to the surface $E_{\perp}$ exhibits a phase shift close to 180° and hence the sum of the

incident and reflected electric field is approximately zero [4]. As a consequence, the infrared light polarized in the surface plane cannot activate a molecular vibration and in analogy with this a molecule can only absorb infrared light if the change of dipole moment has a component in the plane of incidence, perpendicular to the surface, Figure 3.2. This is called the surface selection rule. Therefore it is common to use p-polarized light ($E_{\perp}=0$), i.e., light with an E-vector perpendicular to the surface. The polarization of the light will increase the surface sensitivity since the background noise is reduced.

3.2 Quartz Crystal Microbalance

The quartz Crystal Microbalance (QCM) is based on the piezo electric effect, e.g. an applied pressure on a piezo electric material generates an electric potential between the deformed surfaces or vise versa [5]. Thus by applying an alternating voltage to two electrodes deposited on each side of the crystal an oscillation of the crystal will be initiated. Cutting of the crystal along different crystallographic directions will influence the deformation oscillations. The so-called AT-cut results in shear deformation of the crystal with stable and sharp resonance frequency. If metal films, in the present case iron, are deposited on the electrodes and subsequently exposed to an atmosphere, they will form corrosion products on the surface. In Figure 3.3 an illustration of an oscillating crystal is shown, where λ_i represents the wavelength for the resonance oscillation with and without corrosion products. The resonance frequency can easily be measured and λ_i calculated. λ_i is proportional to the thickness and the mass of the coated crystal and hence the mass of the corrosion products can be calculated by comparing the frequency before and after the formation of corrosion products.

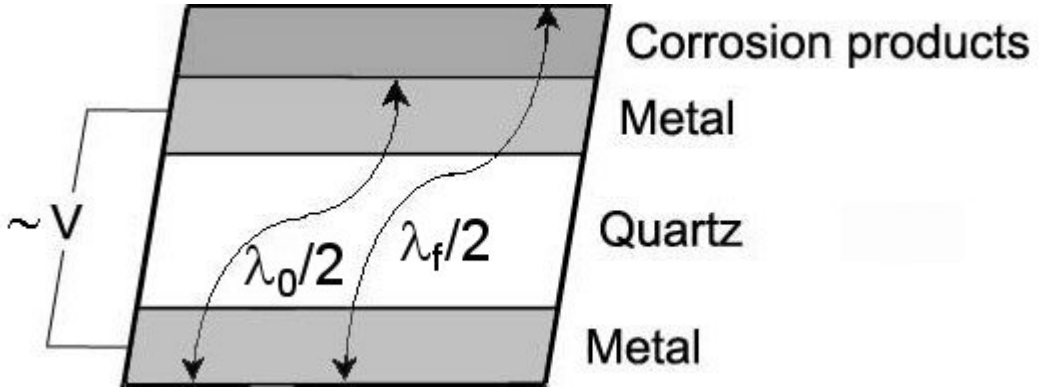

Figure 3.3. Schematic picture of an oscillating crystal. λ_f and λ_0 represents the wavelength for the oscillation with and with out corrosion products.

By using the Sauerbrey equation, it is possible to correlate the change in crystal resonance frequency with a change of mass of the deposited iron film [6]:

$$\Delta f = - \frac{2 f_0 \Delta m}{\rho_q \nu_q} \qquad (3.1)$$

where Δf is the frequency shift, f_0 the resonance frequency at the start of the experiment, Δm the mass change per area, ρ_q the density of quarts and, ν_q the shear wave velocity of quarts. A change of 1 Hz corresponds to a mass change of approximately 18 ng/cm^2 for a 5 MHz crystal. This is less than the mass of an adsorbed monolayer of water [7]. The equation is derived assuming that the density and shear wave velocity are the same for all materials, e.g. metal electrode, corrosion products and quartz crystal. This assumption is valid if the thickness of the quartz crystal is order of magnitudes larger than the metal and corrosion products. Our iron films are in the order of a few 1000 Å thick, while the quartz crystal is approximately 1 mm thick. The Sauerbrey assumption also implies that the different layers are rigid, homogeneous and has good adhesion. This is not obviously valid for water or other liquids adsorbed on a surface. However, Rodahl and Kasemo [8] showed that the Sauerbrey equation could be used up to 0.1 µm thick water films with high accuracy. But as reported in paper V even thicker water films can locally be formed when aerosols are present on the surface,

consequently great care has to be taken when using QCM in less well defined environments.

The main advantages with QCM are that it can be used at atmospheric pressure and can measure mass changes less than a monolayer with high accuracy and high time resolution. Some drawbacks are the lack of lateral resolution, the inability to distinguish between different species causing a mass change and sensitivity to pressure and temperature changes in the atmosphere.

3.3 IRAS/QCM and Optical Microscopy/QCM

The combined IRAS/QCM experimental set up consists of an FTIR spectrometer with external detector, a QCM sensor probe with corresponding frequency counter, a corrosive air generation and analysis system and an exposure chamber. The FTIR spectrometer with detector allows scanning over the frequency range (4400 cm^{-1} down to approximately 500 cm^{-1}) where many metal oxides and corrosion products can be found and the QCM sensor probe can detect sub monolayer amounts of water or metal oxides. The gas generation/analysis system can at the present handle corrosive gases containing humidity, SO_2, O_3 and NO_2, which are some of the most important corrosion stimulators in the atmosphere. In addition well controlled amounts of NaCl crystallites may be deposited *in-situ* on the surface. In Figure 3.4 a cross section of the exposure chamber with the QCM sensor probe and IR beam path is depicted.

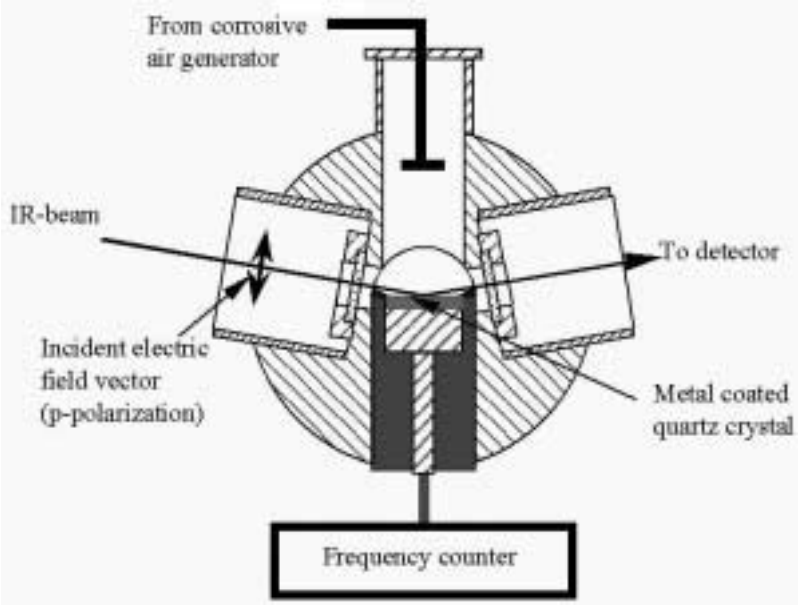

Figure 3.4. Cross section of the exposure chamber, showing the path for the IR-beam, the QCM sample and the corrosive gas inlet.

In order to enhance the surface sensitivity the beam is p-polarized and the angle of incidence is approximately 80° from the sample normal.

In order to be able to achieve structural *in-situ* information of the localized atmospheric corrosion an optical microscope was integrated with a QCM. The experimental set-up is very much like the combined IRAS/QCM (Figure 3.5). It consists of an airtight reaction chamber with well-controlled atmosphere connected to the same gas analysis and gas generation equipment as the IRAS/QCM chamber. The chamber comprises an optical microscope, which enables observations of the metal-coated QCM sample during reaction. It is thereby possible to obtain both kinetic and topographic *in-situ* information. The airflow rate in the reaction chamber was chosen to be the same as in the IRAS/QCM chamber.

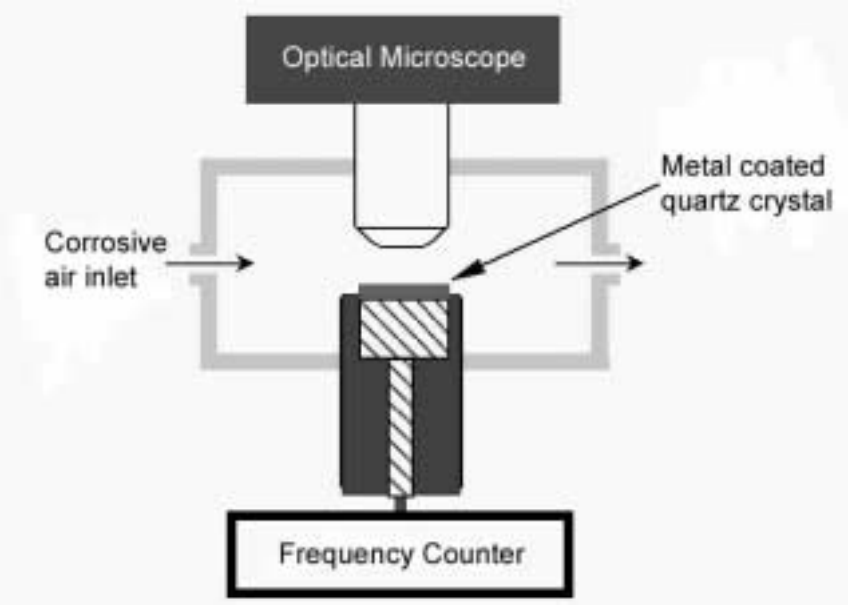

Figure 3.5 Combined *in-situ* optical microscope and QCM

3.4 Scanning Probe Microscopy

A wide variety of so called scanning probe techniques utilizing different interacting forces with a scanning tip for imaging the surface properties have been developed from the ideas of Binning and Rohrer [9]. Two examples are the original idea of the scanning tunneling microscope (STM) and the atomic force microscope (AFM) in which the very weak van-der-Waals forces between the probing tip and the surface are used.

3.4.1 Scanning Tunneling Microscopy

The scanning tunneling microscope was developed by Binnig and Rohrer [10] in the early 1980's and has since evolved into one of the most powerful locally probing tools of surface science. This technique can be used under a wide range of pressures, from ultrahigh vacuum (UHV) up to above atmospheric and it can even be used in liquids. The principle of the microscope is fairly simple, based on the quantum mechanical tunneling mechanism. When a bias voltage, V_{bias}, is applied, the Fermi levels of the tip and the sample are not aligned anymore, electrons are attracted and may

tunnel between the tip and the surface, thus creating a tunneling current, I_t. Depending on the voltage, the electrons are either tunneling into the sample or out of the surface. To be able to accomplish tunneling into the sample empty electron states are needed. Similarly, filled sample states are needed to produce a tunnel current from the sample to the tip.

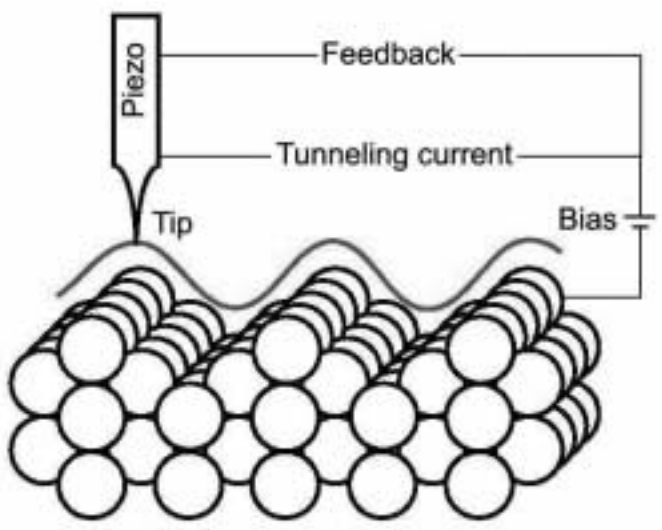

Figure 3.6 Schematic illustration of the principles of operation of the STM.

A schematic illustration of the principles of operation of the STM is shown in Figure 3.6. The sharp probing tip is brought to within a few Å from the sample surface by a piezo driven slider. The high precision piezo drives controls the fine motion of the tip. The extreme sensitivity of the tunneling current to the separation between the sample and the tip, typically one order of magnitude for each Ångström change in distance, presents a way to measure surface corrugations on an atomic scale. Two different operation modes to acquire data are possible. Acquisition at constant current, (z=f(x,y), Constant Current Imaging or CCI)) or at constant height (I=f(x,y), Constant Height Imaging or CHI). In CCI, z is continuously adjusted over the surface to keep the current constant. While in CHI, the feedback loop is disconnected and the current is directly recorded at each point on the surface. The advantage of the CHI operation mode is that it is much faster than the CCI. However, it requires a much flatter surface, and therefore a better quality of the surface. All STM images presented in this thesis were recorded in CCI mode.

The tunneling current is not only a function of the geometric surface structure but is strongly affected by the local electronic structure at the particular tunneling spot. The tunneling current is in fact a representation of the local density of states (LDOS) on the sample at the Fermi level convoluted with the probing state at the end of the tip, which of course is in turn influenced by the geometric structure. These contributions, the geometric and electronic, may in some cases be separated from each other by applying different voltages and thus involving different electronic states in the tunneling process. On an atomic scale, the maxima appearing in an image might even be of a complete electronic character, located in positions not directly corresponding to the location of the surface atoms.

It may be argued that the electron energies typical for STM experiments (ca 1 eV) may not be high enough to resolve individual atoms since the corresponding wavelength is larger than typical interatomic distances in solids of about 3Å [11]:

$$\lambda = \frac{12.3}{E_{eV}} \text{Å} \qquad (3.2)$$

However, the STM is operated in the so-called near field regime where the distance between the tip and sample surface is comparable to or less than the electron wavelength. In this regime, the spatial resolution, which can be achieved, is no longer diffraction limited and is not determined by λ [9,12].

A fundamental parameter for the resulting STM image of a surface is the state of the tip. Information of the atomic and electronic structures of the tip during acquisition is generally unknown, but it is not always crucial as long as the tip is stable during a sufficient period of time. To obtain high resolution both the overall shape and the nature of the apex of the tip are of crucial importance. Therefore good control of the manufacturing process of the tip is required. Modifications of the tip structure do not always have to

be a problem, but one can actually benefit from these changes. A different tip, chemical and/or geometrical, may give an opportunity to probe states that are inaccessible with the normal tip configuration [13].

The first theoretical attempts to calculate the full three dimensional STM current, was based on first order perturbation theory in a transfer Hamiltonian by Tersoff and Hamann [14,15]. Here, the interaction between the tip and the sample has to be sufficiently small to be neglected. A weakness in their model is its inability to calculate atomic resolution on close packed surfaces. The main reason for this is the simplified model of the tip, for which they use a spherically symmetric s-wave function. The problem with atomic resolution was partly solved by the introduction of p and d states in the tip wave function [16]. Still, the corrugations predicted by the calculations of the tunnel current in the case of close packed metal surfaces, and especially the Al(111) surface, were too small. It was later shown by Doyen [17,18], that the interaction between the tip and the sample surface must be taken into account, at least for metallic surfaces.

In scanning tunneling spectroscopy the spectroscopic properties of STM is used. For zero applied voltage the Fermi levels of the tip and sample are equal at equilibrium. When a bias voltage V_{bias} is applied to the sample, the main consequence is a rigid shift of the energy levels downward or upward in energy by an amount $|eV_{bias}|$, depending on polarity. For negative sample bias, the net tunneling current arises from electrons that tunnel from the occupied states of the sample to the unoccupied states of the tip and the opposite when changing polarity. By varying the amount of the applied bias voltage, one can select the electronic states that contribute to the tunneling current and, in principle, measure the local density of states. Feenstra have showed that the normalized quantity $(dI/dU)/(I/U) = (d\ln I)/(d\ln U)$ reflects the electronic density of states reasonably well by minimizing influence of the tip sample separation [19].

3.4.2 Atomic Force Microscopy

In 1986, Binnig *et al.* [20] invented the Atomic Force Microscope (AFM), which enables investigations of non-conducting materials. The principle of AFM, similar to STM, is that a small tip scans the surface. The tip can either be in constant contact with the surface, contact mode AFM, or the cantilever holding the tip may oscillate with a frequency in the range 10-400 kHz with the tip position in intermittent contact or not in contact with the surface, so called tapping mode AFM. The forces acting on the surface are measured and give an image of the topography of the sample. If the sample is a soft material, the tip can cause deformations of the surface. Applying tapping mode AFM will minimize these deformations.

The main advantages of tapping mode AFM are the high lateral resolution down to, in the optimal cases, atomic level obtained at ambient conditions and that the sample is not deformed by the tip.

3.5 Low Energy Electron Diffraction

Determination of surface structures by STM can often be more straightforward by using complementary crystallographic techniques. The most abundant tool in surface crystallography is low energy electron diffraction (LEED). It has, to date, produced over 60% of all solved detailed surface structures and has been extensively described in the literature [21-23]. Determination of an atomic structure with LEED is performed in two steps. First the size, symmetry and rotational alignment of the adsorbate unit cell with respect to the substrate have to be determined. Then, to be able to determine the atomic coordination, a detailed measurement of the diffracted intensities is required.

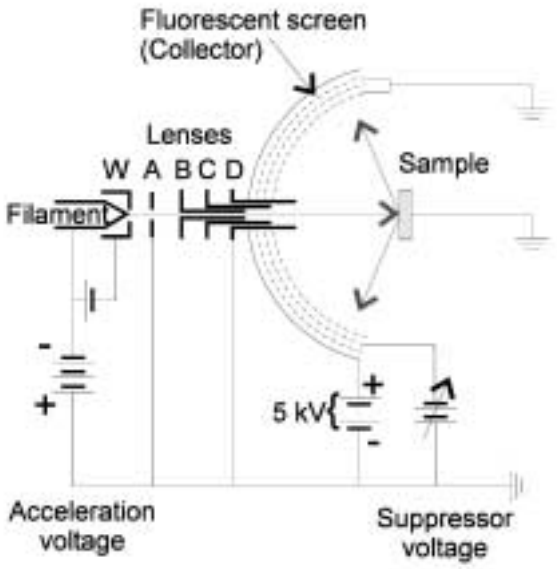

Figure 3.7 Illustration of a low energy electron diffractometer.

A typical experimental set-up is shown in Figure 3.7. A beam of electrons from a gun of a well-defined energy (typically in the range 20-500 eV) is sent normal to the sample surface. The sample is placed at the center of a set of concentric spherical sector grids. The inner grid (closest to the sample) and the sample are grounded to ensure that the electrons leaving the surface are traveling in a field-free space to the grids and thereby maintain their radial geometry. Only the elastically scattered electrons contribute to the diffraction pattern. The lower energy, secondary, electrons are repelled by the energy filtering grids which are set at a potential slightly lower than that of the accelerating voltage of the electron gun. Finally, the transmitted electrons are accelerated towards a fluorescent screen where they produce a LEED pattern.

When a beam of electrons strikes a surface, consisting of repeating arrays of atoms that extend quasi-infinitely in two dimensions, the electron waves diffuse coherently from the two dimensional mesh of atoms and produce a series of intense spots that represent diffraction from all possible parallel rows of surface atoms. The condition for constructive interference is that the change **q** in the wave vector of the scattered electron satisfies [11]:

$$\mathbf{q}\bullet\mathbf{d} = 2\pi\times n, \quad \mathbf{q} = \mathbf{k'} - \mathbf{k}, \text{ n=integer} \tag{3.3}$$

Where **k**, **k'** are incident and scattered electron wave vectors respectively and **d** can be written as:

$$\mathbf{d} = n_1\mathbf{a}_1 + n_2\mathbf{a}_2 \tag{3.4}$$

Where $\mathbf{a}_i$ are the primitive vectors of the direct lattice. The primitive vectors of the reciprocal lattice ($\mathbf{b}_j$) satisfy:

$$\mathbf{a}_i\bullet\mathbf{b}_j = 2\pi\delta_{ij} \tag{3.5}$$

Writing the **q** vector in general form:

$$q = \sum_{i=1}^{3} q_i b_i \tag{3.6}$$

Assigning $\mathbf{b_3}$ to be perpendicular to the surface, the conditions (2.3) and (2.4) require that $\mathbf{q_1}$ and $\mathbf{q_2}$ are integers, while $\mathbf{q_3}$ can be an arbitrary number. Discrete lines in q-space perpendicular to the crystal surface will satisfy these conditions. By introducing the so-called Ewald sphere [11] and a set of lines perpendicular to the crystal surface it is possible to determine the directions of the scattered beams. The Ewald sphere is constructed with its center at a point situated at (**-k**) from the origin of the reciprocal lattice, and with a radius of $|\mathbf{k}|$. In a LEED experiment the direction **k'** of the scattered beams are given by the intersection points of the scattered beams with the fluorescent screen. As a consequence, the diffraction pattern represents the reciprocal lattice of the surface.

As was mentioned above, in order to obtain a constructive interference the range of electron wavelength employed in a LEED experiment has to be comparable to the atomic spacing. Hence, only a few diffraction spots will appear in a LEED pattern. By increasing the incident electron energy, i.e., by

increasing the voltage of the last anode of the electron gun one increases the radius of the Ewald sphere. Therefore, more diffraction spots can be detected as they move towards the (0,0) specular spot. The position of the (0,0) specular spot in the diffraction pattern does not change upon varying the electron energy and results from direct reflection of the primary beam to the surface.

In this thesis, investigating the crystallographic quality of the surface by observing the LEED pattern was often used as a first experimental step in studying the surface. A perfect surface exhibits sharp spots with high contrast compared to the background intensity. Random defects or imperfections will broaden the spots and increase the background intensity due to diffuse scattering from these centers. If facets exist, they will give rise to a secondary LEED pattern with a spot separation different from the normal (0,0) beam. By increasing the electron energy, spots originating from facets move towards a certain position away from the fixed (0,0) position.

3.6 Photoelectron spectroscopy

The experimental technique photoelectron spectroscopy (PES) is based on the photoelectric effect discovered in 1887 by Hertz [24] and described in 1905 by Einstein [25]. In photoelectron spectroscopy, the sample is illuminated by monochromatic light, i.e. photons with a specified energy. The energy carried by a photon may be absorbed through excitations of electrons into higher energy levels. If the photon energy is high enough, electron will be emitted from the sample out into the continuum levels in vacuum and to some extent into the spectrometer [25]. Quantum mechanically, the photoemission is a one-step process where the electron is taken from its ground state to the detector. In order to illustrate and simplify the process it is sometimes described in several steps. In the first step the electron absorbs a photon and is excited from the initial state to a final state within the

crystal with both energy and crystal momentum conserved. In the final state the electron propagates to the surface.

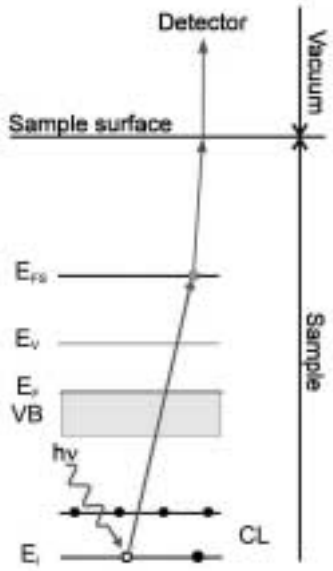

Figure 3.8 Principle of PES

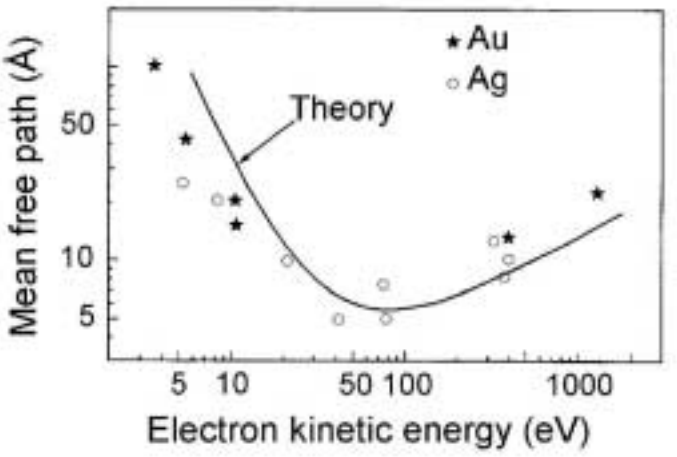

Figure 3.9 The "universal" curve for electron mean free path

On the way to the surface the electron may be inelastically scattered. In this scattering process it will loose information about its initial state, as energy and wave-vector are not conserved. Electrons that are scattered one or several times contribute to a secondary background in the photoemission spectrum. To enhance the surface contribution in a spectrum a high degree of surface sensitivity is desirable and this is one of the more important advantages of synchrotron radiation: the tuneable photon energy. The mean free path (λ) of an electron in a solid varies with its kinetic energy and has a minimum around 50 eV [26]. In order to get the highest possible surface sensitivity the photon energy is tuned so that the emitted electrons from the specific core level of interest have a kinetic energy of about 50 eV. On the low kinetic energy side, the mean-free-path increases as the number of possible excitation events decreases with E_k. On the high kinetic energy side, λ increases due to the shorter interaction times at higher electron velocities. The dominant energy loss mechanisms are the excitation of valence electrons and plasmons. At low energy, valence electron excitations dominate, while plasmon excitations become important above the plasmon energy.

When the electron has reached the sample surface it may escape from the material out into the surrounding vacuum. To do so, its kinetic energy ($h\nu$ - E_B) has to be higher than the vacuum level energy E_V. Its kinetic energy in the solid is then diminished by the work function of the sample Φ_S and becomes E_k. In practice, the analyser and the sample are in electrical contact and their Fermi levels are aligned.

By measuring the intensity of emitted photoelectrons as a function of kinetic energy, an electron distribution curve (EDC) in binding energy is obtained. According to the Kooperman's theorem the kinetic energy of an electron is equal to the photon energy minus the binding energy of the electron, where the binding energy is referred to the vacuum level. In reality Kooperman's theorem is never observed. The main reason for this is the so-called relaxation shift [27]. When the core hole is created, other electrons relax in energy to lower energy states and thereby screen this hole partially. This process will make more energy available to the outgoing photoelectron. In the case of metals, with very mobile valence electrons, the valence electrons will efficiently screen the core hole. This leads to an additional inter atomic relaxations shift and to an increased photoelectron kinetic energy.

In photoemission spectroscopy one often makes a distinction between core levels and valence band states. A core level is an electronic level, which is localized and mainly atomic-like, in contrast to valence levels which are delocalized and participate in the chemical bonding [28]. The binding energy of a core level is dependent on the local electron distribution of valence electrons and hence, also upon the chemical environment, such as bonding to different atomic species or the atom being at the surface where the coordination is different from that in the bulk crystal [29]. The core level shifts are sometimes very small and thus high-energy resolution and good surface sensitivity may be required in order to resolve them.

3.6.1 Analysis of photoelectron spectra

The interpretation of core level spectra is often non-trivial and reveals many of the physical processes affecting the line shape of the core level spectrum. In the analysis, the experimentally obtained spectrum is normally decomposed into one or more components, which represent contributions from different groups of atoms on the surface with different binding energies. The theoretical line shape of separate components is characterized by several parameters: the binding energy, the intensity, the spin-orbit splitting (if not a s-level), and the branching ratio that is related to the occupation of the spin-orbit split components. This value may in reality deviate from the ideal value, due to photoelectron diffraction [30] and different cross-section for the two sublevels, which may substantially influence the intensity.

The theoretical function, or component, is often a so-called Voigt function, i.e., it is a convolution of a Gaussian and Lorentzian function. The Lorentzian width is normally attributed to the lifetime broadening of the core level originating in the finite lifetime of the core hole created in the photoemission process. A finite lifetime will, according to the uncertainty principle, lead to a spread in the electron kinetic energy. The lifetime of the core hole is determined by its decay mechanisms (Auger or radiative). The Gaussian width is thought to take care of all other broadening contributions, such as phonon broadening, limited experimental resolution and inhomogeneties in the surface, giving rise to slightly different binding energies. The effect of phonon broadening can be substantially suppressed by cooling the sample. Finally, if the sample is metallic, the photoemitted electrons may excite electron hole pairs around the Fermi level. As a consequence of this energy loss mechanism metallic samples display an asymmetric (Doniach-Sunjic [31]) line profile with a tail on the high binding energy side. When analyzing spectra using the Donjac-Sunjic line profile it is important to remember that the asymmetry is dependent upon the density of states at the Fermi level.

Moreover, the measured spectrum does not only consist of the core level lines, but the background has to be taken in consideration. As mentioned earlier, inelastically scattered electrons in the solid form this background of secondary electrons with low kinetic energy. Its shape is often approximated by a Shirley function [32].

The energy shift of a core level cannot simply be assigned to the initial valence electron distribution around a particular atom before the excitation. The state of the system when the core electron is extracted and a core hole has been created needs to be accounted for, i.e. final state effects. The system tends to screen the positive core hole; for metallic systems the electron cloud redistributes to take care of the screening, while in dielectric systems the core hole surrounding is polarized so as to compensate for the extra positive charge provided by the hole. The final state effects, as well as the initial state effects, can be different from surface and bulk atoms. Hence, the observed binding energy shift is a combination of initial and final state effects and the observed binding energy is the difference in total energy for the system with and without the core hole.

References

1. P. R. Griffiths and J. A. DeHaseth, *Fourier Transform Infrared Spectroscopy*, John Wiley & Sons, New York (1986)
2. K. Nakamoto, *Infrared and Raman Spectra of Inorganic and Coordination Compounds*, 4th ed., John Wiley & Sons, New York (1986)
3. N.V. Richardson and A.M. Bradshaw, *Symmetry and Electron Spectroscopy of Surfaces, in: Electron Spectroscopy: Theory, Techniques and Applications*, Vol. 4, Eds. Baker and CR. Bundle, Academic Press, London (1980)
4. M. Alonso and E. J. Finn, *Fundamental University Physics, Volume II, Fields and Waves*, 2nd ed., Addison-Wesley Publishing Company, Massachusetts (1983)

5. A. W. Czanderna and C. Lu, *Application of Piezoelectric Quartz Crystal Microbalance*, Elsevier, Amsterdam, The Netherlands (1984)
6. G. Sauerbrey, *Z. Phys.*, **155**, 266 (1959)
7. D. W. Rice, P. B. P. Phipps and R. Tremoureux, *J. Electrochem. Soc.*, **127**, 563 (1980)
8. M. Rodahl and B. Kasemo, *Sensors and Actuators A,* **54,** 448 (1996)
9. R. Wiesendanger, H.J. Guntherodt, *Scanning tunneling microscopy II,* Springer Series in Surface Science 28, Springer Verlag (1992)
10. G. Binnig, H. Rohrer, Ch. Gerber and E. Weibel, *Phys. Rev. Lett.*, **49**, 57 (1982)
11. N.W. Ashcroft and N.D. Mermin, *Solid state physics*, Saunders Collage CBS Publishing, Philadelphia (1988)
12. R. Wiesendanger, *Scanning probe microscopy and spectroscopy: metods and applications*, Cambridge University Press (1994)
13. B.J. McIntyre, P. Sautet, J.C. Dunphy, M. Salmeron, G.A. Somorjai, *J. Vac. Sci. Technol. B,* **12**, 1751 (1984)
14. J. Tersoff and D.R. Hamann, *Phys. Rev. Lett.*, **50**, 1998 (1983)
15. J. Tersoff and D.R. Hamann, *Phys. Rev. B,* **31**, 805 (1985)
16. C.J. Chen, Phys. Rev. Lett., **65**, 448 (1990)
17. G. Doyen, D. Drakova and M. Scheffler, *Phys. Rev. B,* **47**, 9778 (1993)
18. G. Doyen, E. Koetter, J.P. Vigneron and M. Scheffler, *Appl. Phys. A,* **51**, 281 (1990)
19. R.M. Feenstra and J.A. Stroscio, *Phys. Scripta T*, **19**, 55 (1987)
20. G. Binnig, C. Quate and C. Gerber, *Phys. Rev. Lett.*, **56**, 930 (1986)
21. M.A. van Hove, S.Y. Tong, *Surface Crystallography by LEED*, Springer-Verlag, Berlin (1979)
22. J.B. Pendry, *Surf. Sci Rep.*, **19**, 191 (1993)
23. M.A. van Hove, *Surf. Interface Anal.*, **28**, 36 (1999)
24. H. Hertz, Ann. Phys., 31, 983 (1887)
25. A. Einstein, Ann. Phys., 17, 132 (1905)
26. A. Kahn, Surf. Sci. Rep., 3, 193 (1983)
27. D.P Woodruff, T.A. Delchar, *Modern techniques of surface science*, Cambridge University Press, Cambridge (1990)

28. N.V. Smith and F.J. Himpsel in *Handbook on Synchrotron Radiation*, Vol 1b, Ed. E.E. Koch, North-Holland (1983)
29. A. Flodström, R. Nyholm and B. Johansson, *Synchrotron radiation research: advances in surface and interface science*, Vol. 1 Ed. R.Z. Bachrach, Plenum Press New York (1992)
30. E.L. Bullock, R. Gunnella, C.R. Natoli, R.I.G. Uhrberg and L.S.O. Johansson. MAX-Lab Activity Report 1993, page 108
31. S. Doniach and M. Sunjic, *J. Phys. C*, 3, 285 (1970)
32. D.A. Shirley, Phys. Rev B, 5, 4709 (1972)

4 Synchrotron radiation

The essence of high-resolution spectroscopy is the ability to resolve different components in a spectrum. In order to resolve finer structures and to work with systems with weak signals, a high surface sensitivity and out-standing quality of the light source (monochromaticity, brilliance etc.) and the spectrometer are required. An increased surface sensitivity can be obtained by working at grazing angles and in electron spectroscopy by tuning the energy of the incoming photon, as the mean free path of an electron in a solid varies with its kinetic energy. Synchrotron radiation is a light source that provides all the above listed criteria's and in the following sections, the principles of synchrotron radiation production will be presented.

4.1 Principles

In synchrotron radiation storage rings both electrons and positrons have been used, but the vast majority of the light sources employ electrons. The electrons are circulated in an orbit and synchrotron radiation is emitted when the electrons are accelerated, to be exact when they experience a change of momentum. When an electron is moving in a circular orbit at a non-relativistic speed, i.e. much slower than the speed of light ($v << c$), the angular distribution of the emitted radiation is as illustrated in Figure 4.1a [1]. The distribution pattern is that of an oscillating dipole or a classical antenna. At a relativistic speed of the electrons ($v \approx c$) the emission will be subjected to a Lorentz transformation and the angular distribution of the emitted intensity will be strongly distorted into a narrow cone in the instantaneous direction of motion of the electron and the emitted spectrum

will be strongly Doppler-shifted (Figure 4.1b). The generation of a continuous spectrum extending from the microwave to hard x-rays can be explained by considering the harmonics of the frequency of revolution, which is in the microwave range. The relativistic transform of the radiation pattern from the electron rest frame into the laboratory frame leads to a distribution of intensity into higher harmonics of the revolution frequency. An increase in the electron energy will give rise to higher harmonics content and thus higher energy storage rings will have enhanced intensity at shorter wavelengths. At high revolution frequencies the density of lines merge into a continuum. Further, since there is a spread in the revolution frequency the spectrum can be considered as white at short wavelengths. Still, the strong polarization of the dipole radiation remains.

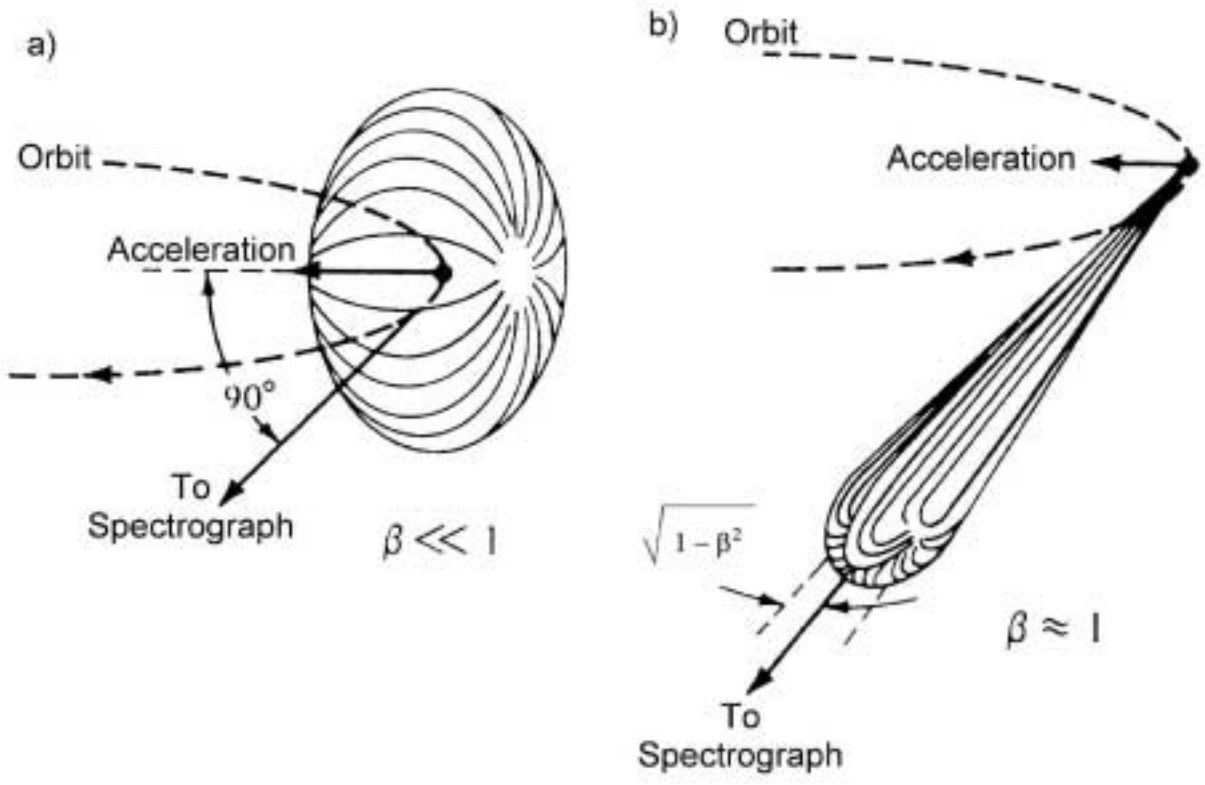

Figure 4.1 Geometries for synchrotron radiation emission, a) slow electrons ($\beta = v/c << 1$) and b) relativistic electrons ($\beta \approx 1$). From [2].

The benefits of synchrotron radiation in spectroscopy are many. Here are some of the outstanding properties listed:

- The wavelengths emitted form an intense continuous spectrum, as shown in Figure 4.2.
- High degree of collimation
- Completely linear polarization in the plane of orbit
- Elliptical polarization above and below the plane of orbit
- High brilliance of the source
- A pulsed time structure in the pico-second range with a very stable intensity
- High stability of the electron beam
- Clean environment (UHV)

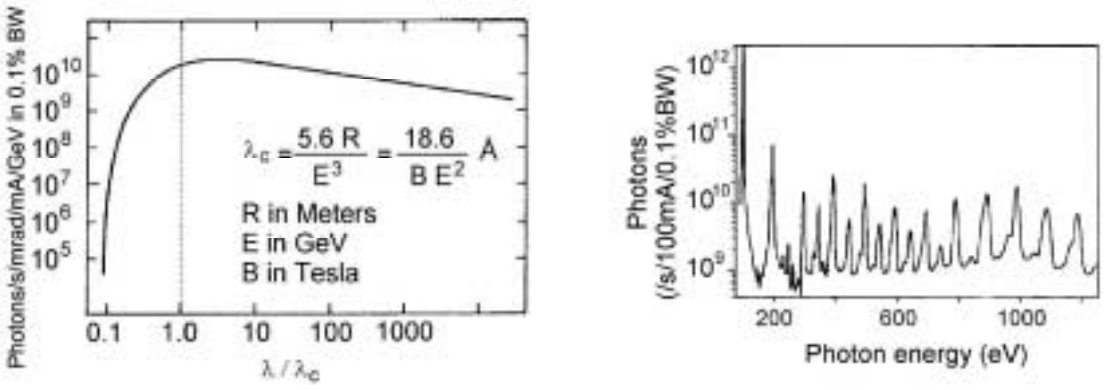

Figure 4.2 a) The spectral distribution obtained by a bending magnet is given by the "universal curve" [3], with λ_c = 5.4 and 41.3 Å for Max II and I respectively (left), b) undulator spectrum (right) [4].

4.2 Insertion devices

As described in the previous section, bending magnets change the electron momentum and give them a curved trajectory and thus synchrotron radiation is created. In third generation synchrotron radiation sources another possibility to create synchrotron radiation is used. So-called

insertion devices, such as wigglers, multipole wigglers or undulators create the light in the straight sections of the rings. A wiggler is a magnetic structure, which forces the electron beam to follow a trajectory with a smaller local radius of curvature than in the bending magnets by using a larger local magnetic field. The effect of the wiggler on the emitted spectrum is to decrease the critical wavelength (λ_c) and thus to shift the overall spectrum to higher energies. The multipole wiggler is composed of several wigglers in series. The transverse oscillations of the electrons are large enough so that the related angular deviation α is wider than the natural opening of synchrotron radiation (γ^{-1}). Therefore, the emitted pulses are not able to interfere and the total intensity obtained is the incoherent sum of the contribution from each wiggler [5]. As a consequence a huge improvement of the photon flux is obtained (Figure 4.3).

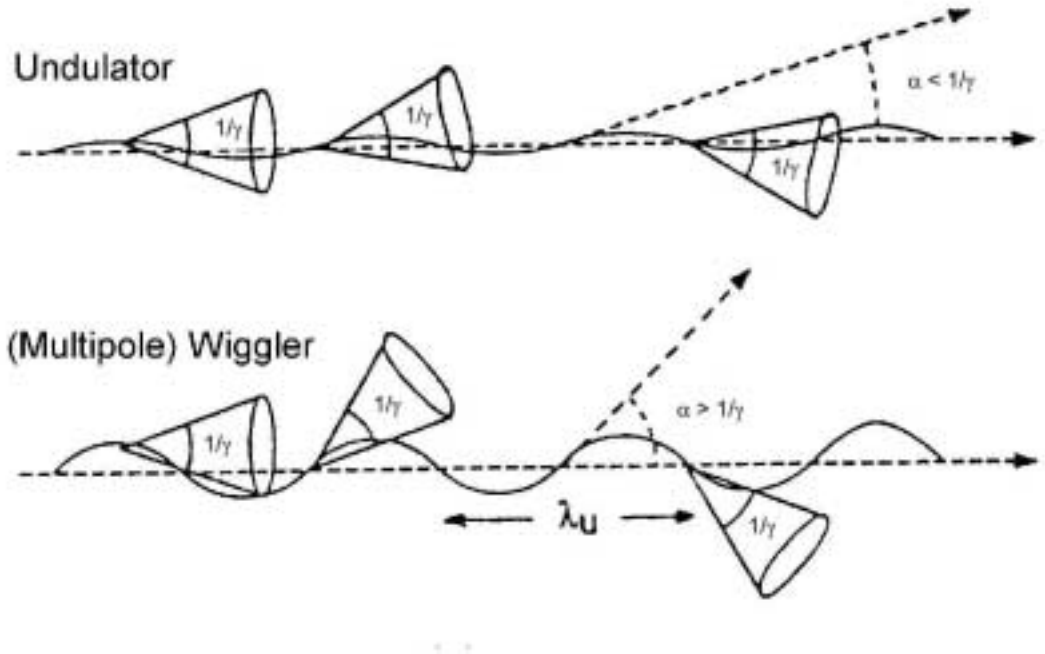

Figure 4.3. Schematic pictures (Top view) of the undulator and multipole wiggler, λ_u is the period of oscillation, $1/\gamma$ the radiation divergence and α the angular deviation. From [2].

In contrast to wigglers that use strong magnetic fields, undulators require rather weak ones. The undulators are designed for a production of quasi-monochromatic light. As for the multipole wiggler, a periodic electromagnetic

structure gently leads the electrons to oscillate transversally in a given plane (planar undulator) or to describe a helix along its mean path (helical undulator). But in contrast to the multipole wiggler the angular deflection of the beam is now kept smaller or equal to the natural radiation divergence angle of synchrotron radiation (Figure 4.3). A beamline on the axis of the undulator receives the radiation emitted along the whole device. The amplitudes of the field radiated at each period of the particle trajectory may thus interfere, resulting in a periodic radiation field. The resonant wavelengths depend on the magnetic field on the axis of the undulator and the electron oscillation periodicity. It is therefore possible to tune the wavelength by tuning the magnetic field strength. This is done by changing the gap between the undulator magnets. Figure 4.3b shows a typical spectrum obtained with the undulator at BL I511, with an opening gap of 23mm [4].

A schematic overview of MAX-Lab is given in Figure 4.4. The main magnetic elements are indicated. The straight sections in MAX II are numbered from 1 (injection point) to 10.

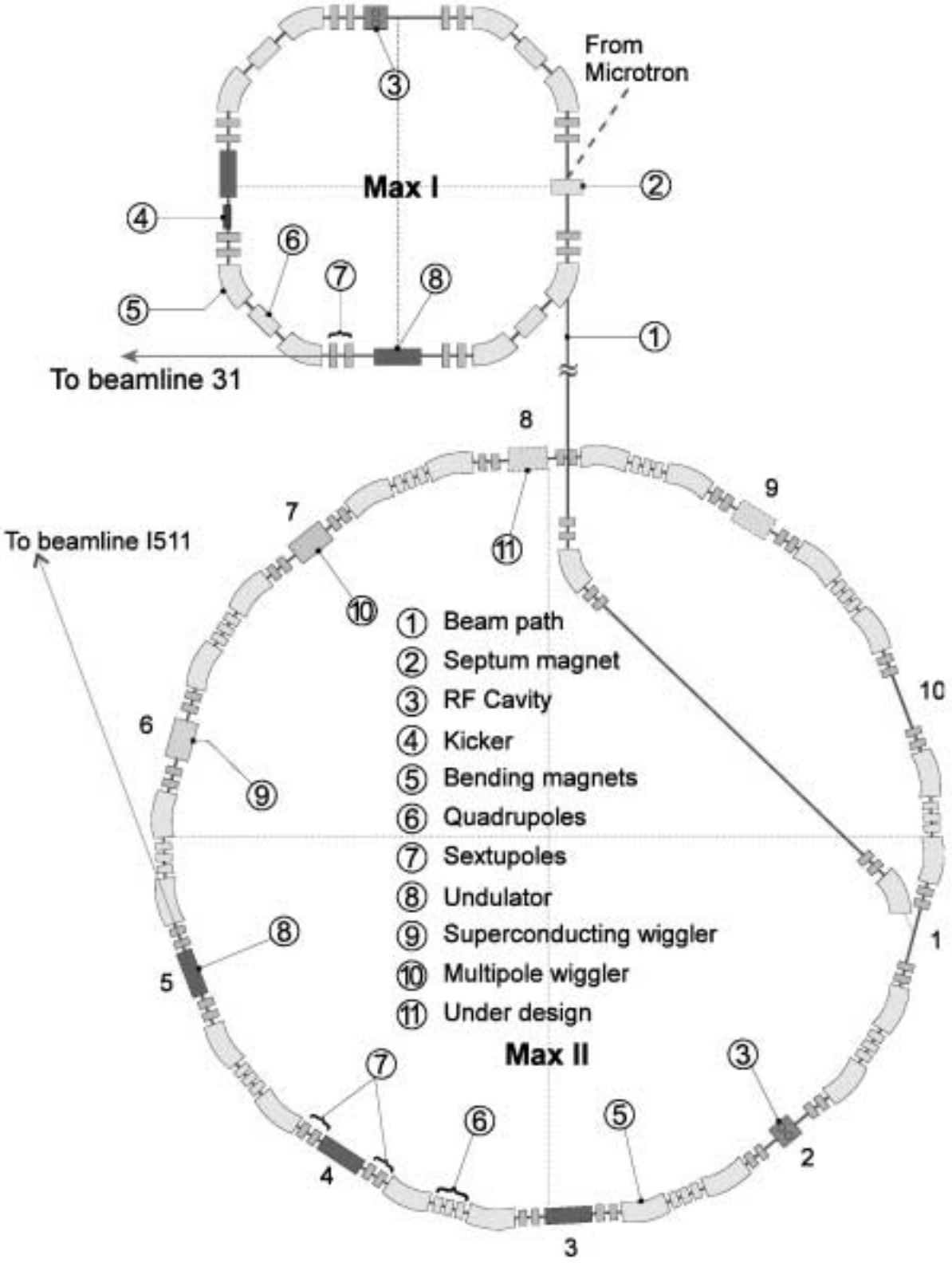

Figure 4.4 Schematic view of MAX-lab.

References

1. D.H. Tomboulian and D.E. Hartman, *Phys. Rev.*, **102**, 1423 (1956)
2. E.E. Koch, D.E. Eastman and Y. Farges, *Handbook on Synchrotron Radiation*, Vol 1a, North-Holland (1983)
3. J. Schwinger, *Phys. Rev.*, **70**, 1912 (1949)
4. R. Denecke, P. Väterlein, M. Bässler, N. Wassdahl, S. Butorin, A. Nilsson, J.E. Rubensson, J. Nordgren, N. Mårtensson and R. Nyholm, *J. Electron. Spectrosc. Relat. Phenom.*, **101-103**, 971 (1999)
5. D. Raoux, *Neutron and synchrotron radiation for condensed matter studies*, Vol. 1: *Theory, instruments and methods*, Eds. J. Bachurel, J.L. Hodeau, M.S. Lehmann, J.R. Regnard and C. Schenkler, Springer-Verlag (1993)

5 Summary of papers

5.1 Paper I

Investigation of the Surface Phase Diagram of Fe(110)-S

Investigations of the interaction of sulfur with iron surfaces is interesting, because Fe-S overlayers have been reported to be corrosion protective in certain environments [1]. Sulfur is also known to play an important role in atmospheric corrosion and catalysis [2].

In the present paper different previously not presented reconstructions and overlayer structures of the Fe(110) surface at different sulfur coverage are shown by atomically resolved STM combined with Auger electron spectroscopy (AES) and LEED. The S concentration on the surface was changed by annealing the Fe(110) single crystal to approximately 700°C for different time periods in order to induce S segregation from the bulk. The first observed reconstruction was Fe(110)c(6x4)-S and this was followed by (3x1) and (1x1) reconstructions. Surprisingly, the previously reported Fe(110)p(2x2)-S reconstruction could not be found within the set of experiments. In the (1x1) reconstruction S occupies the 4-fold site, except close to missing rows in the (1x1) structure where S is shifted to 3-fold sites. At S coverage above one monolayer a (2x1) super structure was formed on top of the Fe(110)(1x1)-S structure. When increasing the coverage further, S grows in a zigzag formation from step edges across the terraces. These zigzag rows grow in the $[1\bar{1}1]$ and [001] directions and form a quasi ordered parallelogram structure. This quasi-ordered structure consists of

parallelograms ordered with an approximate periodicity of 23 Å and 15 Å, oriented along the [001] and $[1\bar{1}1]$ directions.

5.2 Paper II

Oxygen structures on Fe(110)

In this paper the adsorption of oxygen on a Fe(110) single crystal was studied by means of high resolution photoelectron spectroscopy (HRPES) and STM. The photoemission core levels were investigated in detail on both clean and adsorbate covered surfaces. The clean surface showed a distinct shoulder on the high binding energy side of the Fe $2p_{3/2}$ core level. This shoulder was interpreted as a bulk component, since its relative intensity to the main component was independent of adsorption on the surface. The observed shift between the main line and the shoulder was in the order of 0.8 eV. The origin of the multiple components could be interpreted as an exchange split of the final state due to interaction between the $2p$ and $3d$ electrons. In analogy with this interpretation the sublevels were treated with a Zeeman like analysis using equidistant m_j sublevels with equal asymmetry, Gaussian and Lorentzian width. The best fit to the data was found at an equidistant energy spacing of 0.35 eV, <10 % of the spin-orbit split, and thus the Zeeman description can be assumed to be fairly well adapted.

In an attempt to validate the Zeeman assumption, calculations of the energy split using the mean field approximation were performed. According to mean field theory the exchange field of iron is [3,4]:

$$B_E = \lambda M_S = \frac{3k_B T_C}{Ng^2 s(s+1)\mu_B^2} M_S \approx 10^3 T \qquad (5.1)$$

The Zeeman split can be calculated from [5]:

$$\delta E = g\mu_B m_j B \qquad (5.2)$$

$$g = 1 + \frac{j(j+1) - l(l-1) + s(s+1)}{2j(j+1)} \qquad (5.3)$$

The corresponding energy shift between the m_j sublevels is then:

$$2 \times \delta E \approx 10^{-1} eV$$

After adsorption of oxygen (2x5), (2x2) and (3x1) reconstructions were observed with atomically resolved STM. The iron surface was further exposed to gradually higher doses of oxygen. Deconvolution of the O 1*s* HRPES spectra revealed two components shifted approximately by 0.4 eV. The component at lower binding energy dominates at low coverage, while the high binding energy component increases in intensity with increasing O coverage. The formation of oxides was observed in the Fe 2*p* spectrum in the region between 709 eV and 711 eV. Further, well-ordered iron oxides were grown by exposure to oxygen at 250 °C. The O 1*s* core level contained a single component with a binding energy similar to that of the high binding energy component in the just discussed O 1*s* spectrum. LEED and STM images of this structure showed a large Moiré pattern with a 22.1 Å x 30.9 Å unit cell.

5.3 Paper III

Initial oxidation of Fe(100) and Fe(110)

The initial adsorption of oxygen and the subsequent oxidation of different single crystal iron surfaces was the main focus of this study. Fe(100) and Fe(110) single crystals were studied by means of high resolution photoelectron spectroscopy and LEED at both room temperature and elevated temperatures.

The Fe(100) showed faster oxidation rate than Fe(100), both at room temperature and 300°C. At room temperature both surfaces initially form oxide layers with iron mainly in the form of Fe^{2+}, but at higher doses the formation of Fe^{3+} is observed. The Fe^{3+} formation is presumed to occur at the gas/oxide interface. During oxidation at 300°C the oxidation pattern is reversed and the initial oxide is formed mainly by Fe^{3+} ions. At higher coverage, oxides with Fe^{2+} ions become the more dominant oxidation products.

The line profile of the Fe $2p_{3/2}$ core level from the clean Fe(110) and Fe(100) surface show evidence for multiple components in the peak. Investigations with plane polarized light with different polarization relative to the sample surface showed a dichroism structure with four different components. Theses components were interpreted as m_j sublevels and were found from the dichroism structure and subsequent curve fitting to have an equidistant energy spacing of approximately 0.45 eV.

5.4 Paper IV

Photoelectron microscopy of filiform corrosion of aluminum

In this paper *in-situ* IRAS and photoelectron spectroscopy/microscopy was combined to study the initial atmospheric corrosion of aluminum. To our knowledge it is the first time this combination has been used with an objective to study atmospheric corrosion.

The aluminum samples were investigated during and after exposure to well-controlled amounts of NaCl (approximately 50 μg/cm²) and humidified air at 90% relative humidity. The deliquescence of NaCl crystallites could be followed *in-situ* at high relative humidity (IRAS), as well as the growth of different aluminum oxide, hydroxide and chloride corrosion products. Scanning electron microscopy and energy dispersive x-ray analysis after exposure showed corrosion products formed like filaments and chlorine

enrichment in the filament heads. As the exposed samples were further investigated with synchrotron based photoelectron microscopy and spectroscopy, spectra taken of the Al 2*p* core level showed an intricate structure with multiple components in the core level. In the microscopy mode the distribution of the different components could be mapped over the surface. These mapping images revealed an enrichment of, what we expect to be, aluminum chloride containing compounds in the heads of the filaments whereas aluminum oxides/hydroxides were observed both inside and outside the filaments.

5.5 Paper V

In-situ studies of filiform corrosion of iron

In this paper the influence of small amounts (~ 2 μg/cm^2) of deposited NaCl crystallites on the initial atmospheric corrosion of iron was investigated. The investigations were mainly performed *in-situ* at different relative humidity. Deliquescence of the NaCl crystallites and formation of corrosion products was followed at a relative humidity ≥75% with QCM combined with either IRAS or optical microscopy. The deliquescence of the NaCl crystallites was found to be fast, in the order of seconds.

The nucleation rate of localized corrosion was remarkably enhanced compared to only exposure in humidified air and the resulting corrosion attacks initiate at droplets of NaCl solution. The corrosion product morphology on a NaCl exposed surface is different from surfaces only exposed to gas phase corrodents. The NaCl-induced corrosion products grow in approximately 10 μm wide filaments, characteristic of filiform corrosion.

During progress of filiform corrosion specific features observed include a constant mass increase rate with time at a given relative humidity, an NaCl-depleted radial zone in front of the active filament head, chloride transport towards the filament head that is mass-transport limited, a chlorine-

enriched filament head, a filament growth that is driven by a differential aeration cell within the filament, and a step-wise growth of the filament head.

In all, filiform corrosion under present conditions was found to proceed in steps, driven by a differential aeration cell, and growing by mass transport limited chloride ion transport towards the filament head, which resulted in successive formation of new anodic and cathodic sites.

5.6 Paper VI

In-situ studies of the initial atmospheric corrosion of iron

This paper deals with the initial atmospheric corrosion of iron under the influence of humidified air and corrosive gases. The presented results show that an aqueous adlayer of constant mass was physisorbed on the surface at a given relative humidity. A linear relationship between the absorption intensity in the water bands (IRAS) and the mass change (QCM) could be established. The aqueous adlayer was found to be thicker when compared to previous studies performed on copper. In the presence of a thick water layer, at high relative humidity, an absorbance band at 1100 cm^{-1} was observed that disappeared when dry air was introduced. This absorbance band seems to be strongly connected to the presence of water on the surface.

When introducing 200 ppb SO_2 no significant increase in reaction kinetics could be observed. But after additional introduction of 200 ppb O_3, the formation of sulfate surface species could be monitored quantitatively with monolayer sensitivity and a significant increase in reaction kinetics could be discerned. The results were compared with similar studies on copper and great difference in atmospheric corrosion behavior was recognized. The protective film on iron is initially more corrosion resistant than on copper and in contrast to copper, iron does not form a homogeneous film with corrosion products. When the protective film of iron fails, atmospheric

corrosion attacks occur on narrow areas of the iron surface, in contrast to copper that forms a uniform film. The mass gain of iron during current exposure in relative humidity, SO_2 and O_3 is about 20 times lower than of copper.

5.7 Paper VII

Comparison of the early stages of corrosion of copper and iron investigated by in situ TM-AFM

In this study we have used tapping mode atomic force microscopy (TM-AFM) in the investigation of the early stages of atmospheric corrosion of pure copper and iron. By using this method information of changes in the topography of the sample surfaces with emphasis on the shape and lateral distribution of the corrosion products grown within the first 1300 min of weathering was gathered.

A completely different mechanism of the initial stages of the atmospheric corrosion of copper and iron could be observed. In the case of copper, an uniform growth of the features was seen during exposure to humidified air (80% relative humidity), whereas the iron surface remained unaltered under these conditions. After introduction of an additional concentration of 250 ppb SO_2 large protrusion were formed on the copper surface in addition to the previously formed homogeneous layer, whereas only very few protrusions occurred on the iron surface. Initiation of a corrosion attack of the iron surface could only be observed after introduction of 250 ppb NO_2, whereby pitting corrosion occurred. With increasing exposure time, protruding corrosion products appeared nearby the pits while main parts of the iron surface still remained intact and did not show any corrosion at all. This is to the authors' knowledge the first time that pitting corrosion of iron could be monitored *in-situ* in a corrosive atmosphere with a sub-micrometer resolution.

5.8 Paper VIII

In-situ studies of sulfate nest formation on iron

In this paper the initial SO_2-induced atmospheric corrosion was followed *in-situ* by three highly surface sensitive and complementary techniques, IRAS, QCM and AFM. The resulting corrosion attack was local in nature and resembled so-called sulfate nests, frequently observed on steel naturally exposed outdoors. The conclusions drawn challenge the established model for formation and growth of sulfate nests: SO_2 alone is not a sufficient prerequisite for sulfate nest formation. Only when an oxidant such as NO_2 or O_3 is added to the corrosive atmosphere, sulfate nests can be detected. The conditions and formation of sulfate nests are discussed in view of all in-situ observations generated.

Iron has been exposed to humidified air with additions of SO_2 alone or in combination with either NO_2 or O_3. The resulting atmospheric corrosion effects have been followed in-situ with IRAS, QCM and AFM, all with a surface sensitivity corresponding to less than a monolayer of corrosion products. The following conclusions could be drawn: Upon exposure to humidified air with 90% relative humidity, iron forms a gel-like film causing a mass increase that originates from physisorbed water, monitored by an IRAS absorbance band at 1100 cm^{-1}, and from a mixture of iron oxide and -hydroxide.

When introducing 200 ppb SO_2 into the humidified air, no change in corrosion effects could be discerned by any of the techniques used. The result bears clear evidence that iron under present conditions is passive against SO_2, a conclusion that contradict the established model for formation of sulfate nests. Only when oxidants, such as NO_2 or O_3, are introduced into the SO_2-containing humidified air, localized corrosion attacks can be detected, similar to what previously has been reported and described as sulfate nests. This corrosion form is autocatalytic and observed

together with a rapidly increasing corrosion rate, caused by dissolved Fe^{2+} ions, which promote the catalytic conversion of SO_2 to sulfate, which increases sulfate-induced dissolution of iron, which creates more Fe^{2+} ions etc. The sulfate nests seem to spread laterally through enhanced deposition of SO_2 at cathodic sites, due to high pH, which lowers the pH and creates new anodic sites, which creates new cathodic sites, etc. When NaCl is deposited on iron, filiform corrosion occurs upon exposure to humidified air. Introduction of SO_2 inhibits the corrosion rate, whereas SO_2 + NO_2 has an accelerating effect. In this case local pits are formed, without any scale covering the pits, at some distance from the filiform corrosion features. The absence of a scale over the pits suggests a corrosion attack that is different in nature from sulfate nests, which are assumed to operate through the presence of a semi-permeable membrane covering the pits.

References

1. L.-G. Johansson, *SO_2 induced corrosion of carbon steel in various atmospheres and dew point corrosion in stack gases*, Thesis, Chalmers University of Technology, Sweden (1982)
2. G.A. Somorjai, *Introduction to surface chemistry and catalysis*, John Wiley & Sons, New York (1994)
3. C. Kittel, Introduction to solid state physics, Seventh edition, Wiley, Brisbane (1996)
4. N.W. Ashcroft and N.D. Mermin, *Solid state physics*, Saunders Collage CBS Publishing, Philadelphia (1988)
5. E. Merzbacher, *Quantum Mechanics*, Second edition, John Wiley & Sons (1970)

6 Contributions of the candidate

I have had a central part in all the planning, data acquisition and analysis presented in this thesis. In all papers except paper VII I have been responsible for preparing a first version of the papers/manuscripts.

7 Future work

It would be interesting to extend the investigations of the iron surface with X-ray absorption and emission studies. These investigations are possible to perform at atmospheric pressures with well-defined samples and would provide new *in-situ* information about the formation and chemical composition of the protective film formed on iron surfaces.

Another interesting project would be to continue the STM studies and perform high-pressure and high-temperature investigations of oxygen and water adsorption on single crystal iron oxides. The interaction of chloride ions with the iron protective film is not yet fully understood and an increased knowledge in this area would also be most valuable for the understanding of the breakdown mechanism of passive films. Moreover, investigation of the interaction between nitrogen and iron as well phosphor and iron would be of great technological importance.

Photoelectron microscopy/spectroscopy investigations of filiform corrosion of iron will most likely provide new information that may provide an improved understanding of the subject.

Further, more detailed studies of the interaction of SO_2 with NO_2 and O_3 would be most interesting, as well as high resolution scanning Kelvin probe measurements of localized corrosion.

8 Acknowledgements

First of all I would like to thank my supervisors Prof. Ulf Karlsson and Prof. Christofer Leygraf for believing in me from the start and giving me full freedom to develop my interest in surface science.

I am in great debt to my supervisor in practice, Dr. Mats Göthelid with whom I have had the privilege to work with at campus, Lund and finally here in the suburb. You have really taught me a lot and thanks for all our conversations about something and everything.

I also want to express my sincere gratitude the following people (in no specific order) that have in one way or the other supported me during the time of this thesis:

- Dr. Christoph Kleber, for all your patient work with the AFM and for the beers in Krems. It was really a pleasure working with you.
- Prof. Manfred Schreiner, for inviting me to a wonderful time in Vienna.
- Prof. Guy LeLay, thank you for all your comments and the time in Lund as well as Chamonix.
- Dr. Torbjörn Åkermark, for always being friendly and in a good mood. All the papers you have provided me with and the valuable discussions we have had during the years have really helped me a lot.
- Dr. Oscar Tjernberg, for all discussions about photoemission and other contemporary issues of our society.
- Dr. Ted Aastrup, thank you for always answering all my questions and for introducing me to the IRAS and QCM techniques.

- I want to thank Dr. Gunnar Hultquist for all the different discussions we have had and for the interest you have shown in my research.
- Dr. Inger Odnevall-Wallinder for all the time you spent at the ESCA.
- Sofia Bertling for all the struggle with the SuCoSt project.
- The pasta mafia for all the delicious lunch breaks: Anna, Erik and Daniel.
- To all my roommates over the years: Martin, Magnus, Thomas, Bo and Mohammad. Thank you for being so easy to get going with and such good friends.
- The support from the staff at MAX-lab is also kindly acknowledged.
- In addition I want to thank all@matphys.kth.se and all@corrosci.kth.se for creating such a friendly atmosphere.

I would like to thank Prof T. Suzuki and Prof. K.V Rao for introducing me into the field of science during my stay in Japan and back home in Sweden. From my stay in Japan, I also want to thank Dr. Yusuke Itoh. It was really fun working with you and I hope we meet again soon.

The Swedish Research Council (VR) and the Göran Gustafsson Foundation is gratefully acknowledged for funding.

Finally, I would like to thank my friends and family:

Anna, Hank, John, Micke, Peter, Paul, Ronnie och alla andra...

Mamma, Pappa och Johanna. Tack för allt hittills.